iopscience.iop.org

Effect of resonant magnetic perturbations on COMPASS-C tokamak discharges

This content has been downloaded from IOPscience. Please scroll down to see the full text.

View the table of contents for this issue, or go to the journal homepage for more

Download details:

IP Address: 128.62.18.33
This content was downloaded on 12/03/2015 at 15:38

Please note that terms and conditions apply.

1992 Nucl. Fusion 32 2091

EFFECT OF RESONANT MAGNETIC PERTURBATIONS ON COMPASS-C TOKAMAK DISCHARGES

T.C. HENDER, R. FITZPATRICK, A.W. MORRIS, P.G. CAROLAN, R.D. DURST*,
T. EDLINGTON, J. FERREIRA, S.J. FIELDING, P.S. HAYNES, J. HUGILL,
I.J. JENKINS, R.J. La HAYE**, B.J. PARHAM, D.C. ROBINSON, T.N. TODD,
M. VALOVIČ, G. VAYAKIS
AEA Fusion, Culham Laboratory,
UKAEA-Euratom Fusion Association,
Abingdon, Oxfordshire, United Kingdom

ABSTRACT. Experimental results from the COMPASS-C tokamak reveal a sharp threshold in amplitude above which externally applied static resonant magnetic perturbations (RMPs) induce stationary magnetic islands. Such islands (in particular, $m = 2$, $n = 1$ islands) give rise to a significant degradation in energy and particle confinement, suppression of the sawtooth oscillation and a large change in the impurity ion toroidal velocity. The observed threshold for inducing stationary (2,1) islands is consistent with a phenomenological resistive MHD model which takes into account plasma rotation (including poloidal flow damping) and externally applied resonant fields. Broadly similar results are found for applied fields other than $m = 2$, $n = 1$. Other results from RMP experiments are also discussed, such as the stabilization of rotating MHD activity, stimulated disruptions and extensions to the disruptive density limit. Finally, the likely effect of field errors on large tokamaks is briefly examined in the light of the COMPASS-C results.

1. INTRODUCTION

In the past, several tokamak experiments have used coils external to the plasma to produce static resonant magnetic perturbations (RMPs). The aim of this type of experiment is generally to control and influence magnetohydrodynamic (MHD) instabilities, in particular those with a poloidal mode number $m = 2$ and a toroidal mode number $n = 1$, which usually precede major disruptions. In the PULSATOR tokamak, application of a ramped (2,1) RMP field was found initially to stabilize rotating MHD activity, but at higher applied fields disruptions were stimulated [1]. For discharges close to the density limit, results from the TOSCA tokamak indicated a modest improvement (about 15%) in the density limit due to the application of a (2,1) RMP field [2]. In the TOKOLOSHE tokamak, application of large helical fields resulted in locking of pre-existing rotating modes, leading eventually to disruption of the plasma [3]. In this paper, we present results from the COMPASS-C [4, 5] tokamak which further clarify the effect of RMP fields. We then interpret these seemingly diverse experimental observations in terms of a phenomenological resistive MHD model which takes into account external perturbations and plasma rotation (including poloidal flow damping).

2. EXPERIMENTAL SET-UP

2.1. Introduction

The results presented here were obtained during the first phase of the COMPASS experiment (COMPASS-C). During this phase, a thin circular vacuum vessel of relatively low aspect ratio was employed (major radius R = 0.557 m, minor radius of limiter a = 0.2 m, plasma current $I_p \leq 200$ kA, toroidal field strength $B_\phi \leq 1.75$ T, a 0.7 mm bellows section stainless steel vessel of minor radius $r_W = 0.22$ m with a theoretical vessel time constant $\tau_{m=1} \approx 60\,\mu$s). A graphite poloidal ring limiter was used, and midway through the experiments presented in this paper a boron-carbon layer was applied by boronization to the inside of the vacuum vessel [6].

In the following, we employ the convention that a $(+m, n)$ perturbation (where m and n are positive integers) has a helical pitch in the same sense as that of the equilibrium magnetic field, and a $(-m, n)$ perturbation has a pitch in the opposite sense. A $(+m, n)$

Permanent affiliation:

* University of Wisconsin, Madison, WI, USA.

** General Atomics, San Diego, CA, USA.

perturbation is 'resonant', provided that a flux surface with a safety factor $q_s = m/n$ lies within the plasma. Otherwise, it is 'non-resonant', as are all $(-m, n)$ perturbations. In describing the various RMP configurations, the Fourier analysis is based on a 'geometric' (i.e. not corrected for the variation of field line pitch around flux surfaces) poloidal angle measured with respect to the centre of the vacuum vessel.

2.2. Description of RMP saddle coils

COMPASS-C was equipped with a large number of saddle coils which were installed outside the vacuum vessel at a radius $r_C = 0.278$ m (centred on $R = 0.576$ m) and could be connected together to give a wide variety of different RMP fields (see Fig. 1). These saddle coils consisted of ten toroidally directed bars with an angular extent of 70° in each quadrant, with poloidal links which could be changed between discharges, and were powered by two independent waveform controlled amplifiers. Saddle coils in two toroidally opposite quadrants could be configured to give a predominantly $n = 1$ field with the $\pm m$ components of equal magnitude. Henceforth, we shall refer to such a configuration as a 'non-helical' configuration. Alternatively, coils in all four quadrants could be used to give a 'helical' configuration, in which either the $+m$ or the $-m$ components were dominant.

In this paper we mainly concentrate on COMPASS-C RMP configurations for which the (2,1) harmonic was dominant, and the poloidal sidebands, $m = 1$ and 3, were minimized (typically, $b_{r(3,1)}/b_{r(2,1)} \sim b_{r(1,1)}/b_{r(2,1)} \lesssim 0.1$ in vacuum, for $r \sim a$, where b_r is the perturbed radial field strength). Although the exact harmonic mix varied, all helical (2,1) RMP configurations referred to in this paper gave $b_{r(2,1)} \sim 14$ G at $r = a$ when the RMP coil current (I_c) was 1 kA. Some results for configurations with dominant harmonics other than (2,1) will also be discussed. One configuration used in COMPASS-C (the so-called 'crescent' configuration) was designed to mimic a horizontal displacement of a poloidal field coil, and so had the broad Fourier spectrum characteristic of an error field [7] ($b_{r(3,1)}/b_{r(2,1)} \sim b_{r(1,1)}/b_{r(2,1)} \sim 0.9$ in vacuum, at $r = a$). Mimicking of a horizontal displacement was achieved by using a toroidally directed RMP bar situated close to a poloidal field coil in order to effectively null out part of its current and then energizing a bar situated in the same quadrant, but slightly further away from the field coil, with equal and opposite current. Bars were configured in a similar manner in two adjacent quadrants, and in the opposite manner in the two remaining quadrants, to give a dominant $n = 1$ field.

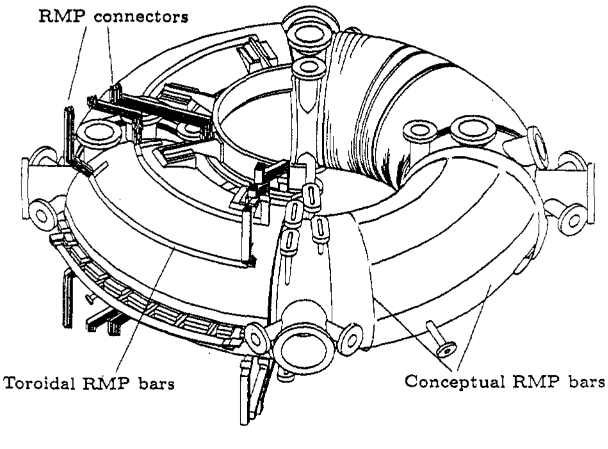

FIG. 1. View of COMPASS-C, showing the RMP configuration. The left hand quadrant shows the toroidal bars and connections from the torus (to patch boards above and below the machine, allowing the connections of the toroidal bars to be varied). The right hand quadrant shows a conceptual view of the paths of the RMP bars.

2.3. Description of magnetic diagnostics

Within the vacuum vessel at a radius $r_M = 0.21$ m there were 20 equally poloidally spaced pickup coil packages, at each of three toroidal locations ($\phi = 0°$, 67.5°, 180°). Each package contained a radial (b_r), poloidal (b_θ) and toroidal (b_ϕ) field pickup coil. In order to ensure that the effects of the applied RMP fields were not masked by error fields, great care was taken in COMPASS-C to minimize field errors during assembly. This was achieved with the aid of 16 high sensitivity coil packages measuring the horizontal (b_R) and vertical (b_Z) fields (centred at $R = 1.1$ m and $Z = -0.16$ m). The poloidal field coils were shifted, tilted, and their ellipticity adjusted in situ, in order to minimize the field errors relative to the toroidal field coil axis, with the result that total error fields below 0.5 G for $n = 1$ ($< 5 \times 10^{-5} B_\phi$) were achieved [8]. Subsequent to assembly, the b_R elements of these high sensitivity coil packages were used to detect stationary magnetic islands. We shall refer to these as the 'small' locked mode detectors. Four large saddle loops, straddling the outboard midplane (at $r = 0.296$ m, with poloidal extent 33° and toroidal extent 57°), were also used to detect stationary islands. We shall refer to these as the 'large' locked mode detectors.

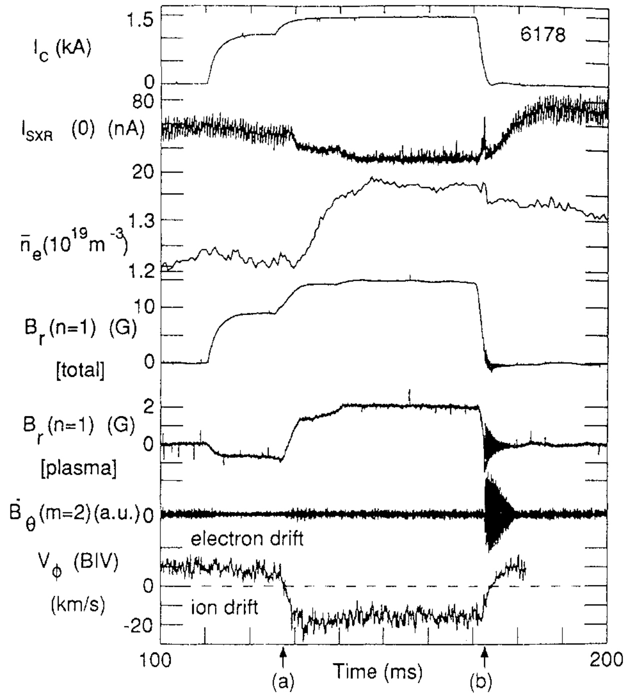

FIG. 2. Typical Ohmic COMPASS-C discharge in which application of a (2,1) RMP causes 'mode penetration'. The diagnostic data shown are the RMP saddle current (I_c), a central horizontal SXR chord (I_{SXR}), the line averaged electron density ($\bar{n}_e$), the total $n = 1$ signal at the large locked mode detectors, the $n = 1$ 'plasma' signal at the large locked mode detectors, the $m = 2$ poloidal field ($\dot{b}_\theta$) signal, and the boron IV impurity ion toroidal velocity. Mode penetration occurs at the time marked (a), and unlocking (and subsequent 'spin-up') occurs at the time marked (b).

3. EXPERIMENTAL RESULTS AND THEIR INTERPRETATION

In this section we discuss the COMPASS-C RMP results and their theoretical interpretation. We begin the presentation of the experimental results by examining a discharge which exhibits many of the key RMP effects produced by application of a helical (2,1) RMP field. Figure 2 shows the RMP saddle current (I_c), the central soft X-ray (SXR) chord, the line averaged electron density ($\bar{n}_e$), the $n = 1$ total and 'plasma' locked mode (b_r) signals, the $m = 2$ poloidal field ($\dot{b}_\theta$) trace, and the boron IV impurity ion toroidal velocity, for an ohmically heated discharge during the current flat-top ($B_\phi = 1.1$ T, $I_p = 98$ kA, $q_\psi \sim 4.3$). The 'plasma' locked mode signal is obtained by subtracting the $n = 1$ vacuum field measured by the large locked mode detectors in a separate vacuum shot from the $n = 1$ field measured by the same detectors in the presence of plasma.

It can be seen that the 'plasma' locked mode signal indicates the sudden growth of a large stationary mode at $t \sim 128$ ms (marked (a) in Fig. 2). We shall refer to this event as 'mode penetration'. We always observe a significant confinement degradation associated with mode penetration of (2,1) RMPs, as well as complete suppression of the sawtooth oscillation, and a large change in the impurity ion toroidal velocity. Another effect invariably associated with penetration is an increase in the volume averaged plasma resistivity signalled by a moderate (about 50%) increase in the loop voltage and a small (about 2%) drop in the feedback controlled plasma current (I_p). Mode penetration has only been observed in COMPASS-C when the applied perturbation is 'resonant'.

As the RMP field is switched off, a large mode can be seen to 'spin up' on the $m = 2$ poloidal field channel and the $n = 1$ locked mode channel (at a time marked (b) in Fig. 2). This mode is subsequently observed to decay away on a time-scale of a few milliseconds.

In Sections 3.1–3.2 we analyse and interpret each of the above mentioned effects. In addition, in Sections 3.3–3.6 we discuss the stabilization of rotating $m = 2$ modes, stimulated disruptions, modifications to the disruptive density limit, and results for RMP fields other than $m = 2$, $n = 1$.

3.1. Mode penetration

3.1.1. Introduction

We interpret the mode penetration event shown in Fig. 2 as the sudden onset of magnetic tearing, resulting in the formation of a stationary (2,1) island. This interpretation is consistent with a phenomenological model of the interaction of RMP fields with rotating plasmas, which is outlined in Appendix A. We propose that, as a result of both viscous and inertial effects, a *rotating* plasma is able to resist the tearing induced by an externally applied RMP field until a critical threshold field strength is exceeded. Plasma viscosity is able to suppress forced tearing because the viscous drag on a static island due to plasma rotation must be balanced by an electromagnetic locking force if the island is to remain stationary. In general, this is not possible until the island exceeds a certain threshold width. Plasma inertia is able to suppress forced tearing in a rotating plasma because the advective inertia of the strongly sheared velocity field in the vicinity of a stationary island has a stabilizing effect which again can only be overcome once the island exceeds a certain threshold width. Estimates for the threshold island width (Eq. (A.24)) and the associated perturbed field strength at the edge of the plasma (Eq. (A.29)) are given in Appendix A. It should be noted that these threshold estimates are based on the requirements of force balance for a state in which only the plasma velocity in the immediate vicinity of the induced island is modified. The dynamics of mode penetration are not addressed by this phenomenological model (presented in Appendix A). An enhanced model which also includes these effects is currently under development [9].

3.1.2. Variation of the mode penetration threshold with density

Figure 3 shows experimental data for a set of discharges with $B_\phi = 1.1$ T, $I_p \sim 95$ kA and $q_\psi \sim 4.5$, plotted in line averaged electron density ($\bar{n}_e$) versus (2,1) helical RMP coil current (I_c) space. We record occurrences of no penetration, penetration, and penetration followed by a stimulated disruption. The helical RMP configuration used in this particular study is such that $I_c = 1$ kA corresponds to $b_{r\,\mathrm{vac}(2,1)} = 13.4$ G at the edge of the plasma ($r = a$). It is clear from the figure that the critical RMP coil current required to induce mode penetration increases with increasing plasma density.

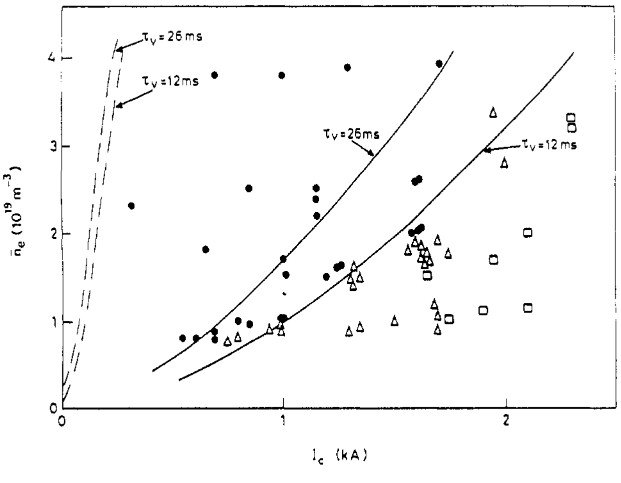

FIG. 3. Data obtained from COMPASS-C RMP discharges with $q_\psi \sim 4.5$, showing occurrences of no penetration (●), penetration (△), and penetration followed by a stimulated disruption (□), plotted in the (2,1) RMP saddle current (I_c) versus line averaged electron density ($\bar{n}_e$) plane. The solid curves are the model predictions for the penetration threshold calculated assuming strong poloidal flow damping for $\tau_\nu = 12$ ms and $\tau_\nu = 26$ ms. The broken curves are the model predictions calculated assuming free rotation for $\tau_\nu = 12$ ms and $\tau_\nu = 26$ ms.

Figure 3 also shows the penetration thresholds predicted by our model calculated for both poloidally flow damped and freely rotating plasmas. The details of this phenomenological model of mode penetration are set out in Appendix A. Our calculations assume vacuum behaviour of the tearing eigenfunctions external to the (2,1) mode rational surface, a model q profile $[q = q_\psi(r/a)^2]$ and a model density profile $[n = n_0\,\{1 - (r/a)^2\}^{1/2}]$. We employ the $\Delta_0'(W)$ relation which is deduced in Section 3.1.4, assuming that Δ_0' is density independent. It should be noted that this $\Delta_0'(W)$ relation is calculated by fitting to experimental data and does not result from a calculation for an assumed current profile. The natural mode frequency f_s (i.e. the frequency of the (2,1) Mirnov activity before the application of the RMP) in these discharges is about 14 kHz and is virtually independent of density. The effective mass number of the fuelling ions, calculated from measurements of the deuterium to hydrogen ratio and Z_{eff}, is about 1.9. The viscosity time-scale τ_ν, estimated from the rate of island spin-up after the RMP is switched off, lies between 12 ms and 26 ms for these discharges (see Section 3.2.5). It should be stressed that no free parameters are used in calculating the model penetration thresholds shown in Fig. 3.

It is evident from Fig. 3 that agreement between the predictions of our model and the experimental data is only possible if the plasma is subject to strong poloidal flow damping (i.e. the velocity shift associated with mode penetration is almost entirely *toroidal* in nature). A previous study of the braking of rotating magnetic islands via interaction with the vacuum vessel in JET also concluded that tokamak plasmas are subject to strong poloidal flow damping [10].

The flow damped model penetration curves shown in Fig. 3 demonstrate that fair agreement with the experimental data is possible within the entire range of estimated τ_ν. For typical COMPASS-C discharges the dominant contribution to our model penetration threshold comes from plasma *viscosity*, with plasma *inertia* contributing only about 10% (see Section A.3). It follows that the observed increase of the critical RMP coil current with plasma density must be attributed to a fairly weak dependence of τ_ν on $\bar{n}_e$. As is discussed in Section 3.2.5, this is consistent with one particular interpretation of our observations of the rate of island spin-up, but a systematic increase of τ_ν with $\bar{n}_e$ cannot be ruled out.

The experimental mode penetration threshold has also been examined for the 'crescent' RMP configuration described in Section 2.2. This configuration is intended to mimic a horizontal displacement of a poloidal field coil and, consequently, has a broad Fourier spectrum. Nevertheless, the critical (2,1) perturbation strength at the edge of the plasma required to induce mode penetration is found to be almost identical with that observed for a predominantly (2,1) configuration. This result shows that the poloidally coupled sidebands have little effect on the penetration threshold.

All of the data shown in Fig. 3 are taken from discharges in which the RMP field was applied during the current flat-top. In a small number of discharges a 'crescent' RMP field was either ramped up with the plasma current or established at a constant level before plasma breakdown. In all such cases, penetration occurred during the current flat-top with the same threshold as in the discharges studied in Fig. 3. This behaviour is understandable because the $q = 2$ surface lies deeper inside the plasma at smaller plasma currents and is therefore less strongly affected by a fixed RMP field strength applied at the edge of the plasma.

3.1.3. *Variation of the mode penetration threshold with edge-q*

We have examined the variation of the mode penetration and stimulated disruption thresholds with q_ψ. The stimulated disruption results are discussed in detail in Section 3.4. In this study the toroidal field is fixed at 1.1 T and the density at $\bar{n}_e \simeq 1.25 \times 10^{19}\,\mathrm{m}^{-3}$, while the plasma current is varied from 72 kA, corresponding to $q_\psi \sim 5.8$, to 130 kA, corresponding to $q_\psi \sim 3.2$.

Figure 4 shows the experimental mode penetration and disruption boundaries over the range of q_ψ. Also shown is the prediction of our model for the mode penetration threshold in a strongly flow damped plasma. The approximations used to calculate the model threshold are as described in Section 3.1.2. We again employ the $\Delta_0'(W)$ relation deduced in Section 3.1.4, assuming that Δ_0' is independent of q_ψ. The natural mode frequency f_s used in calculating the thresholds for these discharges varies from about 17 kHz for $q_\psi \sim 5.8$ to 11.5 kHz for $q_\psi \sim 3.2$. We use a viscosity time-scale of $\tau_\nu = 12$ ms, which is appropriate for the group of discharges in question according to the analysis of Section 3.2.5. It can be seen from Fig. 4 that there is fairly good agreement between the experimental data and our model penetration curve over a wide range of q_ψ. The model curve appears to increase less steeply with q_ψ than the experimental data. This discrepancy can be accounted for if the (2,1) mode becomes slightly more unstable (i.e. Δ_0' increases) as the edge-q decreases.

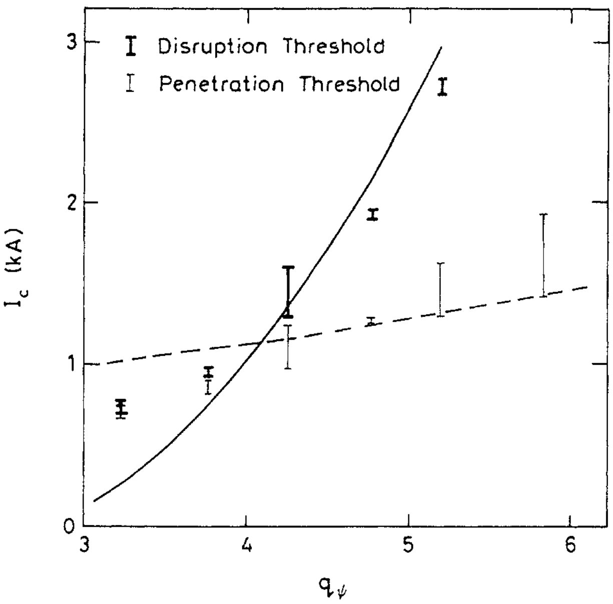

FIG. 4. Variation of the (2,1) penetration and stimulated disruption thresholds with q_ψ for COMPASS-C discharges with $\bar{n}_e \sim 1.25 \times 10^{19}\,\mathrm{m}^{-3}$. The broken curve is the model penetration threshold (calculated assuming poloidal flow damping) using experimentally determined frequencies with $\tau_\nu = 12$ ms, and the solid curve is an empirical fit ($W/(a - r_s) \sim 0.70$) to the disruption threshold.

3.1.4. *Locked mode detector data*

The $n = 1$ 'plasma' locked mode signal in Fig. 2 indicates that the presence of plasma initially *reduces* $b_{r n=1}$ below the vacuum value, but, after the penetration event occurs, $b_{r n=1}$ *exceeds* the vacuum value (i.e. the plasma amplifies $b_{r n=1}$). This effect can be related to the appearance of a magnetic island via a simple MHD model. When there is an applied RMP, but no induced magnetic island, $b_{r(2,1)}$ is zero at the rational surface (see Section A.2). This means that the radial field eigenfunction $b_r(r)$ is everywhere *smaller* than the vacuum eigenfunction, and this difference may be detected outside the plasma. As the island appears, $b_r(r)$ *increases* (see formula (A.30)). This is illustrated in Fig. 5, which shows the three solutions of the low-β cylindrical tearing mode equation in the presence of an RMP: the vacuum solution, the 'untorn' (i.e. no island) solution, and the 'fully reconnected' solution after penetration (see Section A.2).

Figure 6(a) shows the odd-n perturbed radial field before mode penetration (b_R measured at the 16 small

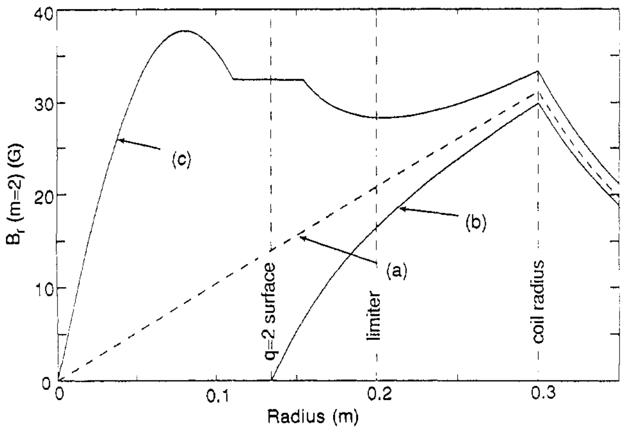

FIG. 5. Typical solutions of the cylindrical tearing mode equation for $J_\phi = J_0(1 - r^2/a^2)^6$, with helical boundary conditions and no conducting wall. The three solutions are: (a) vacuum solution; (b) 'untorn' solution; (c) 'fully reconnected' solution.

locked mode detectors for a discharge with $I_p = 94$ kA, $B_\phi = 1.1$ T, $q_\psi \sim 4.5$) due to an applied (2,1) RMP field, as a function of the toroidal angle (ϕ). The variation of this signal with ϕ is similar to that measured (and calculated theoretically) in vacuum, although the amplitude is reduced by about 8% in the presence of the plasma (see above).

Figure 6(b) shows the incremental step in b_R at mode penetration. It can be seen that the incremental field due to the induced island is predominantly $n = 1$, in marked contrast with the pre-penetration signal which has a substantial $n = 3$ component. Fourier analysis indicates that the incremental signal due to the induced magnetic island is phase shifted by $\Delta\varphi \simeq 31°$, in the electron drift direction, relative to the $n = 1$ component of the pre-penetration signal. This observation accords well with our model of mode penetration (see Appendix A), which predicts a phase shift of the

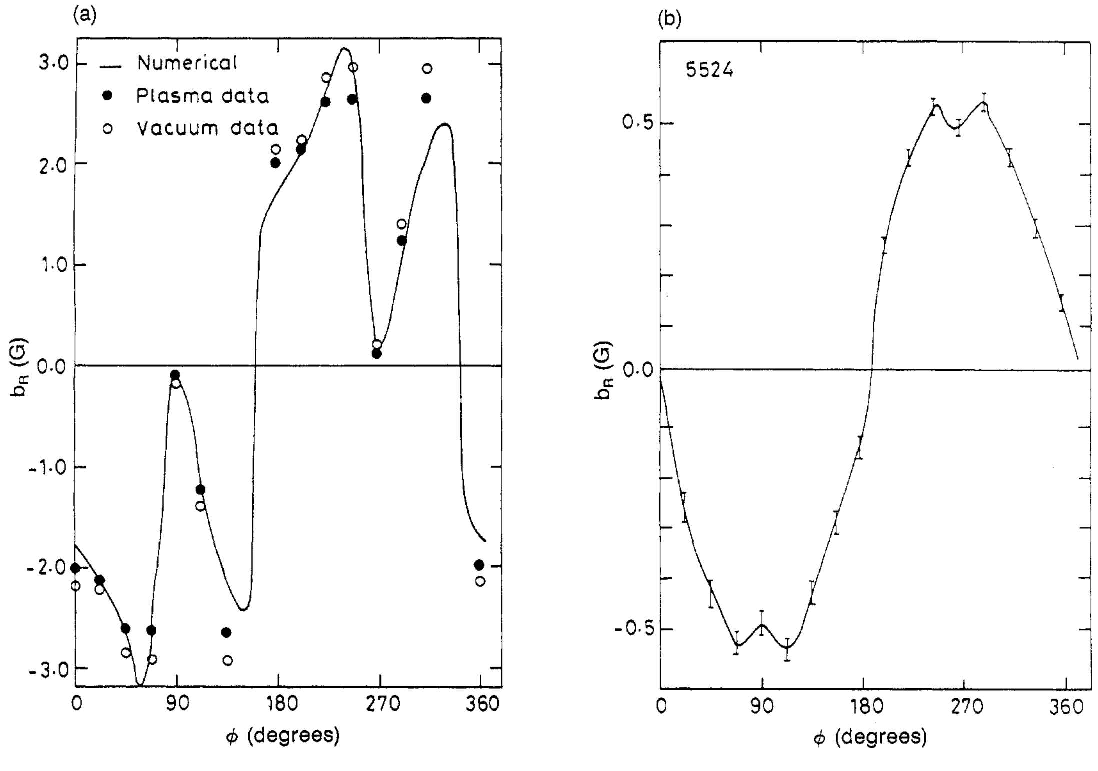

FIG. 6. Toroidal variation of the odd-n radial field (b_R) due to an applied (2,1) RMP, measured at the array of small locked mode detectors. The electron drift direction lies in the direction of increasing toroidal angle (ϕ).
(a) Data from a vacuum shot and from a plasma shot before mode penetration. Also indicated are the expected vacuum values obtained from a numerical simulation of the applied RMP field.
(b) Incremental b_R at mode penetration. The phase of the $n = 1$ component of the pre-penetrated signal (defined as $b_{R_{n=1}} \propto \sin(\phi - \Delta\phi_{n=1})$) is $\Delta\phi_{n=1} \simeq -27°$, whereas the phase of the $n = 1$ component of the incremental signal at mode penetration is $\Delta\phi_{n=1} \simeq +4°$.

stationary island with respect to the applied RMP signal in the direction of natural mode rotation. This phase shift is brought about by the viscous drag of the plasma which applies a torque on the induced stationary island in the direction of natural mode rotation. Our model prediction for the magnitude of the phase shift immediately following penetration (Eq. (A.27)) is about 34° for the discharge under consideration (assuming $\tau_\nu = 12$ ms). Thus, the magnitude of the observed shift agrees fairly well with our model prediction. The direction of the shift is also consistent with our model, since natural modes are observed to propagate in the electron drift direction in COMPASS-C.

The observed amplification of b_R following mode penetration enables us to estimate the equilibrium stability index for stationary tearing modes, Δ_0', since the amplification factor is a function of Δ_0' according to our model (see Section A.2). An estimate of Δ_0' is required for evaluation of the penetration thresholds discussed in Sections 3.1.2 and 3.1.3. In what follows, we make use of a vacuum cylindrical approximation for the mode structure *external* to the rational surface ($r > r_s$). Comparison with solutions of the full cylindrical tearing mode equation indicates that this is a reasonable approximation, provided the rational surface has a radius $r_s/a \gtrsim 0.6$. We also adopt a vacuum q-profile, $q = q_\psi (r/a)^2$, external to the rational surface. It should be noted that this vacuum approximation gives an overestimate of the magnetic shear at the rational surface, and so the island widths we quote are probably slightly underestimated. We estimate that for the discharge under consideration the observed change in b_R at mode penetration corresponds to the formation of a stationary (2,1) island of width $W/a \simeq 0.226$, whereas the expected vacuum island width is $W_c/a \simeq 0.142$. Our model prediction for the initial amplification factor at mode penetration is

$$\frac{W}{W_c} = \left(\frac{2m}{-\Delta_0'(W)r_s}\cos\Delta\varphi\right)^{1/2} \tag{1}$$

(see Eqs (A.6) and (A.8)), where r_s is the radius of the (2,1) rational surface. The above formula implies that $\Delta_0'(W/a = 0.23)a \simeq -2.02$, where use has been made of $r_s = 0.67a$ (from the vacuum q-profile), and $\Delta\varphi \simeq 31°$ (from above).

Before the RMP field is switched on, a saturated (2,1) island of width $W/a \sim 0.025$ is observed rotating at about 14 kHz. Making use of the previously mentioned approximations and the experimental wall time constant (τ_W) obtained in Section 3.2.3, the natural Δ' of a (2,1) mode rotating at a frequency f can be written

$$\begin{aligned}\Delta'(W,f)a &\simeq \Delta_0'(W)a - 2m\left(\frac{a}{r_s}\right)\left(\frac{r_s}{r_W}\right)^{2m} \\ &\quad\times \frac{\lambda^2[1-(r_s/r_W)^{2m}]}{1+\lambda^2[1-(r_s/r_W)^{2m}]^2} \\ &= \Delta_0'(W)a - \frac{0.0142f^2(\mathrm{kHz})}{1+0.0149f^2(\mathrm{kHz})}\end{aligned} \tag{2}$$

where $r_W = 0.22$ m is the radius of the wall, and $\lambda = 2\pi f\tau_W/m$. It follows that, since $\Delta'(W/a = 0.025, f = 14\ \mathrm{kHz}) = 0$ (i.e. the mode is saturated), then $\Delta_0'(W/a = 0.025) \simeq +0.71$. Adopting a simple linear offset form for the variation of Δ_0' with W we conclude, using the inferred values for Δ_0' at $W/a = 0.23$ and 0.025, that

$$\Delta_0'(W)a \simeq 1.04 - 13.3\frac{W}{a} \tag{3}$$

for the discharge under consideration. Note that, since this offset linear form of $\Delta_0'(\mathrm{W})$ is determined by fitting to experimental data, it will implicitly include the linear (in W) saturation term derived in Ref. [11]. We shall see in Section 3.2.4 that this formula is consistent with the observed decay of the induced island after the RMP field is removed.

3.1.5. *Spectroscopic impurity ion rotation*

The impurity ion toroidal velocity during mode penetration has been measured using a high resolution Doppler spectrometer imaging impurity radiation emitted on the plasma outboard midplane. To give good time resolution, the Doppler broadened spectrum of a boron IV line (2821 Å) was split into three photomultiplier channels, each covering approximately one third of the total line width. The photon statistics of this diagnostic ensured a time resolution of about 100 μs. The toroidal velocity was absolutely calibrated by taking measurements in opposite toroidal directions on sequential discharges. During mode penetration, a clear shift in toroidal velocity was observed. This is shown in Fig. 7 for a discharge with $I_p = 98$ kA, $B_\phi = 1.1$ T and $q_\psi \sim 4.3$. It can be seen that the toroidal velocity is slightly reduced by the RMP field, but only changes significantly at mode penetration ($t \sim 130$ ms). The data, which are analysed using an impurity ion temperature derived from the spectral width ($T_{\mathrm{BIV}} \sim 60$ eV), indicate a toroidal velocity shift at mode penetration from an initial value of about

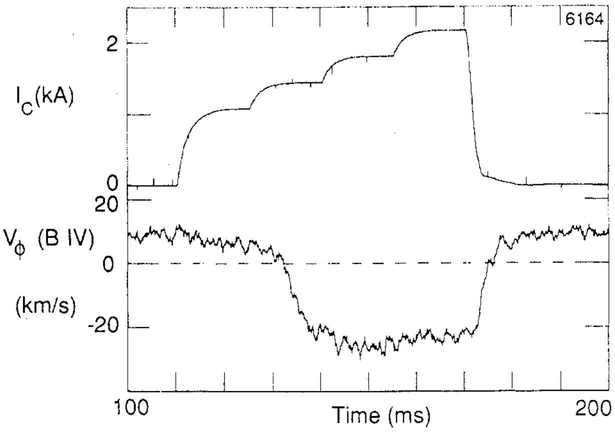

FIG. 7. Typical time variation of the B IV impurity ion toroidal velocity during mode penetration arising from an applied (2,1) RMP.

7 km/s (or 1.5 kHz) in the *electron* drift direction to a final value of about 24 km/s (or 5.3 kHz) in the *ion* direction.

The differential toroidal rotation of a trace ion impurity species with respect to the fuelling ions is governed by the balance of parallel viscous stresses, electrical forces due to the applied loop voltage, and inter-species frictional forces. Using the standard neoclassical result [12] as a guide (with $V_{\text{loop}} \sim 1$ V, $Z_{\text{eff}} \sim 2$–3, $T_i \sim 200$ eV at the centre from neutral particle analyser (NPA) data, implying a typical COMPASS-C ion diamagnetic frequency of the order of 2 kHz in the ion drift direction), we conclude that the B IV ions are unlikely to drift with respect to the fuelling ions by more than about 0.5 kHz in the electron drift direction. It follows that in the unperturbed plasma the fuelling ions in the vicinity of the radiating B IV ions are probably rotating comparatively slowly (about 1 kHz) in the *electron* direction. This implies the presence of an inward pointing radial electric field with an associated central electric potential Φ_0 which is negative with respect to the edge potential. A negative sign for Φ_0 is consistent with previous, more direct measurements [13–17]. The observed $m = 2$ natural mode frequency of about 14 kHz in the electron direction can only be accounted for if the natural mode has a perpendicular velocity *similar* to that of the electron fluid ($T_e \sim 700$ eV in the centre according to a Si(Li) detector, implying a typical COMPASS-C electron diamagnetic frequency of the order of 10 kHz in the electron drift direction). Previous studies have reached broadly similar conclusions [18].

The spectroscopic data indicate an approximately 7 kHz frequency shift of the fuelling ions at mode penetration, whereas the magnetic data show an approximately 14 kHz frequency shift. We have considered two explanations for this discrepancy. Firstly, shear in the toroidal velocity shift profile allows the velocity shifts at the $q = 2$ radius and the radius of the B IV emission to be different. Secondly, a reduction in the electron fluid velocity at the rational surface due to modifications of the electron temperature and density profiles at mode penetration. This would imply a reduced natural mode frequency and, hence, a reduced velocity shift during the penetrated phase.

We firstly consider the effect of toroidal velocity shear in terms of a simple single-fluid model along the lines of the model employed in Appendix A. The basic assumptions underlying the model are, firstly, that the plasma is subject to strong poloidal flow damping, so that only the toroidal component of the fluid velocity is modified at penetration; secondly, that the plasma inside the island separatrix is forced to co-rotate with the island; and thirdly, that the island experiences a zero net (non-electromagnetic) torque when it rotates at its 'natural' (or unperturbed) frequency f_s, but experiences a viscous restoring torque if its frequency differs from f_s. In this model we do not attempt to explain why the island rotates at its natural frequency. It is only the deviation from the natural frequency, induced by electromagnetic torques, which we model. The listed assumptions suggest a single-fluid equation of (angular) motion of the form

$$\rho\frac{\partial\Delta\Omega_\phi}{\partial t} = \frac{1}{r}\frac{\partial}{\partial r}\left[(\rho\nu_\perp r)\frac{\partial\Delta\Omega_\phi}{\partial r}\right] \tag{4}$$

where $\Delta\Omega_\phi(r)$ is the toroidal angular velocity shift (in Hz), $\rho(r)$ is the plasma mass density and $\nu_\perp(r)$ is the anomalous coefficient of perpendicular kinematic viscosity. Velocity shifts at the rational surface are related to island frequency shifts via

$$-n\Delta\Omega_\phi(r_s) = f - f_s \tag{5}$$

where f is the island frequency. The boundary conditions applied to the velocity shift are that $\Delta\Omega_\phi'(0) = 0$ ($' \equiv d/dr$) and $\Delta\Omega_\phi(a) = 0$. The latter condition is equivalent to the assumption that the velocity is clamped at the edge of the plasma (for example owing to direct interaction with the limiter, or charge exchange with neutrals emitted isotropically from the wall). The electromagnetic torque acting on the plasma due to interaction with the RMP is localized within the island region. In the limit in which the finite island width is neglected, a velocity gradient discontinuity must develop at the rational surface in order to provide a localized viscous torque to balance the localized electromagnetic torque during the penetrated phase.

The fluid model described above yields an equilibrium (i.e. $\partial/\partial t = 0$) velocity shift profile following penetration (when $f = 0$) of the form

$$\Delta\Omega_\phi(r) = \begin{cases} \Delta\Omega_\phi(r_s) & r \le r_s \\ \Delta\Omega_\phi(r_s)\dfrac{\ln(r/a)}{\ln(r_s/a)} & r_s < r < a \end{cases} \tag{6}$$

where ρ and $\nu_\perp$ are assumed to be constant across the plasma for the sake of simplicity. Note that the fluid velocity shift is solid-body-like inside the rational surface, but highly sheared outside. The angular velocity shift at the rational surface $\Delta\Omega_\phi(r_s)$ is about 14 kHz (i.e. it is the same as the island frequency shift, for an $n = 1$ mode). This is significantly larger than the observed B IV angular velocity shift $\Delta\Omega_\phi(r_{\mathrm{BIV}})$ of about 7 kHz, where r_{BIV} is the radius of the shell of radiating B IV ions. The velocity shear explanation for this discrepancy is applicable if the shell lies external to the $q = 2$ surface, so that according to Eq. (6) the velocity shift in the vicinity of the shell is less than that at the rational surface. We assume that velocity shifts in our phenomenological fluid give rise to approximately equal velocity shifts in the ion fluid. As is demonstrated in Section 3.2.5, this assumption is consistent with data taken during the spin-up of the induced island after the RMP is switched off. For the discharge under consideration, $\Delta\Omega_\phi(r_s)$ and $\Delta\Omega_\phi(r_{\mathrm{BIV}})$ can be reconciled by the velocity shear explanation if the shell of radiating B IV ions (i.e. the flux surface where $T_{\mathrm{BIV}} \sim 60$ eV) lies at $r_{\mathrm{BIV}}/a \sim 0.82$ (i.e. about 4 cm from the edge). This result is in accordance with estimates from impurity transport modelling which show that the peak B IV emission (282.1 nm) is at 5 cm ± 2 cm from the plasma edge.

An alternative explanation is that the discrepancy between the B IV velocity shift and the shift in mode frequency is due to a reduction in the natural mode frequency f_s during the penetrated phase, brought about by equilibrium profile modifications. This would lead to a global reduction in the velocity shift, since $\Delta\Omega_\phi(r_s) = f_s/n$ following penetration. Given the observed changes in density and confinement at mode penetration, it is likely that some modification of the electron fluid velocity will occur. In fact, the experimental spin-up data suggest a $\lesssim 2$ kHz reduction in f_s during the penetrated phase (see Section 3.2.5), but this is not enough to account for the discrepancy. The explanation based on a change to f_s is also unable to account for the very strong correlation between the mode frequency shift and the B IV velocity shift observed during spin-up (see Section 3.2.5). We conclude, therefore, that the discrepancy between the B IV velocity shift and the shift in the mode frequency is mostly due to shear in the velocity shift profile.

3.1.6. Soft X-ray and vacuum ultra-violet emission

Mode penetration is always accompanied by a substantial reduction in central SXR emission and the complete suppression of the sawtooth oscillation. A comparison of the SXR (energy range 1–10 keV) and line/continuum emission in the vacuum ultra-violet (VUV) (wavelength range 130–150 nm) indicates that part of the observed reduction in the central X-ray emission is due to a decrease in the electron temperature in the plasma core. This is illustrated in Fig. 8, where line integrated profiles in the vertical direction are shown for SXR and VUV emission in two similar shots ($I_p = 110$ kA, $B_\phi = 1.1$ T, $q_\psi \sim 3.8$). The VUV emission (which scales like n_e^2 and has a weak temperature dependence) shows a much smaller drop than the SXR emission (which also scales like n_e^2, but has a much stronger temperature dependence, as is indicated by the stronger central peaking of the pre-penetrated SXR relative to the VUV) when mode penetration occurs. In both cases the emission essentially recovers its pre-RMP level after the RMP field is ramped down ($t > 180$ ms). In general, after the RMP is turned off, the sawtooth oscillation eventually re-establishes itself with the same inversion radius as before mode penetration.

In Fig. 8 the SXR profile over $t = 166$–178 ms (after penetration) shows a slight up-down asymmetry, or 'skew'. The direction of the skew reverses when the direction of the applied saddle current is reversed (i.e. when the phase of the stationary island is inverted). In experiments where the phase of the applied RMP is varied to induce a slowly rotating (about 30 Hz) magnetic island, the direction of the SXR skew is found to co-rotate with the island. This SXR skew is interpreted as a helical displacement of the plasma core associated with the toroidally coupled $m = 1$ sideband of the induced $m = 2$, $n = 1$ island. It should be noted that that q_0 probably does not rise above unity during the penetrated phase. The inversion radius is substantial (about 6 cm) when the sawteeth disappear, and is

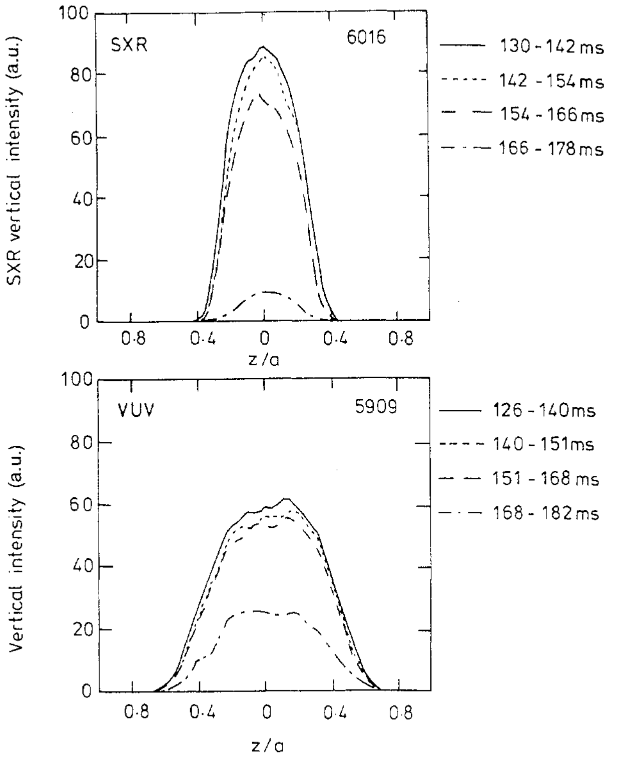

FIG. 8. Typical line integrated vertical SXR and VUV profiles during mode penetration arising from an applied (2,1) RMP. For both discharges, mode penetration occurs at t ~ 168 ms.

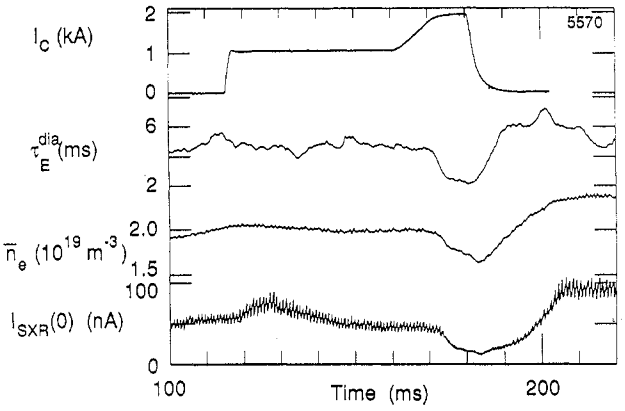

FIG. 9. RMP coil current, diamagnetic confinement time, line averaged electron density and central SXR chord, showing a marked reduction in τ_E at mode penetration (t ~ 170 ms).

about the same when they reappear again after the RMP is switched off.

The $m = 1$ mode in tokamaks is special because it generally lies close to the ideal MHD stability boundary (i.e. $1/\Delta_0' a \rightarrow 0$). In such circumstances the $m = 1$ mode is characterized as an 'internal kink mode' (i.e. a helical displacement of the plasma core) rather than a conventional 'tearing mode'. The stability of the $m = 1$ internal kink mode is not directly related to the tearing stability parameter Δ_0'. The large free energy associated with the nearly marginal $m = 1$ mode allows a strong (O(1) rather than the usual O(a/R)) internal kink sideband of an $m = 2$, $n = 1$ island to develop via toroidal coupling [19]. Before penetration, however, the $m = 2$ RMP field and its toroidally coupled sidebands are restricted to regions lying outside their own resonant surfaces and thus cannot affect the plasma core (see Section A.2). This accounts for the absence of any pre-penetration SXR skew.

3.1.7. Diamagnetic energy confinement

Energy confinement in COMPASS-C Ohmic discharges is well described by the neo-Alcator scaling law (i.e. $\tau_E \propto \bar{n}_e$, leading to T_e approximately independent of density from power balance) [20]. Mode penetration is usually accompanied by a significant degradation in energy confinement. Figure 9 shows the energy confinement time determined from a diamagnetic loop for a discharge in which the RMP current (I_c) is slowly ramped to cause mode penetration (I_p = 94 kA, B_ϕ = 1.1 T, q_ψ ~ 4.5). Such a discharge is chosen in order to avoid rapid changes in I_c which can induce currents in vessel and coil structures and, thus, give rise to spurious signals on the diamagnetic loop. Figure 9 indicates an approximately 50% reduction in τ_E following mode penetration. This cannot be accounted for in terms of the neo-Alcator scaling of τ_E, since $\bar{n}_e$ decreases by only about 15% at penetration. Thus, energy confinement is degraded significantly below neo-Alcator confinement during the penetrated phase. Accordingly, power balance arguments lead us to expect a marked reduction in T_e during penetration. The observed reduction in the plasma diamagnetic energy (about 30%) and the simultaneous increase in the loop voltage (about 50%) during mode penetration (taking into account the behaviour of $\bar{n}_e$ and the lack of variation of the feedback controlled plasma current I_p) are consistent with a 20-30% reduction in T_e, with little overall change in the shape of the temperature profile. The reduction in stored energy (about 30%) is broadly consistent with a model in which the pressure is assumed to be flattened across the (2,1) island [21], although lack of profile data has prohibited a detailed comparison.

3.1.8. Particle confinement and recycling

The edge particle confinement and recycling have been studied during mode penetration using particle balance calculations. The particle confinement time τ_p is determined from the particle conservation equation

$$\frac{dN}{dt} = -\frac{N}{\tau_p} + \rho\frac{N}{\tau_p} + \eta\Phi \tag{7}$$

where ρ is the coefficient of recycling, N is the total number of particles (taken as $N = 2\pi^2 a^2 R\bar{n}_e$), Φ is the gas feed rate and η is the gas utilization efficiency. The quantity η is determined from measurements made separately at constant density ($dN/dt = 0$) and at zero gas feed rate ($\Phi = 0$). Combined with measurements of $\bar{n}_e$ and Φ, this allows the quantity $(1-\rho)/\tau_p$ to be calculated. The quantities ρ and τ_p can then be independently determined by using the measurements of the H_α emission (essentially proportional to the recycling flux $\rho N/\tau_p$), the absolute value of τ_p being determined by normalization to Langmuir probe measurements made before the RMP is applied. The pre-penetration particle confinement time is similar in magnitude to the diamagnetic energy confinement time and exhibits the same neo-Alcator-like increase with plasma density. Analysis of a range of discharges shows that the effect of the RMP on particle confinement and recycling is closely related to the conditioning of the torus.

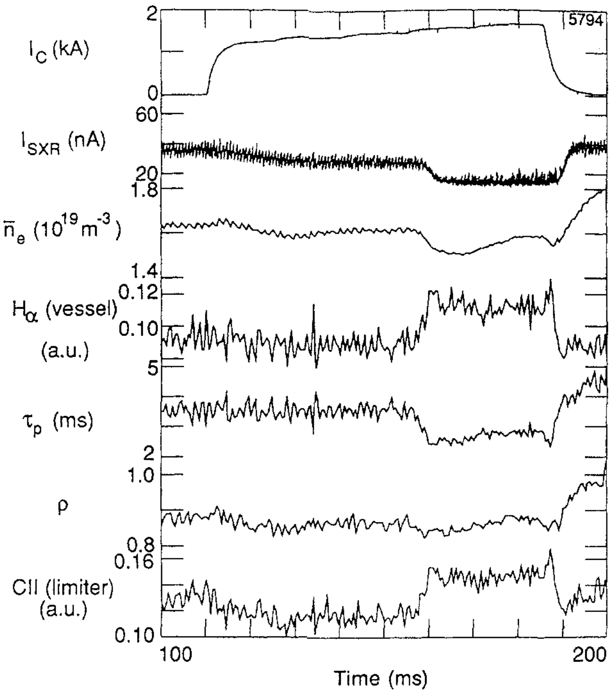

FIG. 10. Typical variation of the H_α emission, particle confinement time (τ_p), coefficient of recycling (ρ) and limiter C II emission, during mode penetration arising from a (2,1) RMP applied to a 'well conditioned' torus.

The results for a typical discharge (I_p = 94 kA, B_ϕ = 1.1 T, $q_\psi \sim 4.5$) with a 'well conditioned' torus (i.e. a torus with relatively clean walls such as might be obtained immediately after helium glow discharge cleaning) are shown in Fig. 10. A clear reduction in the particle confinement time (τ_p) at mode penetration ($t \sim$ 158 ms) is evident. A smaller change in the recycling coefficient (ρ), but not in τ_p, is evident as the RMP is applied ($t \sim$ 110 ms). This small change in ρ occurs in all the discharges examined, but its sign is found to depend on the RMP phase. The H_α observations are made at a location toroidally opposite to the poloidal limiter and gas feed inlet, and represent a view of about 25% of the inside of the torus. In our analysis we assume that the time variation of this relatively localized H_α emission is identical with that of the total recycled flux. Previous measurements show that, in general, for COMPASS-C the total wall and limiter recycling fluxes are approximately equal and have similar temporal variations. The observation that τ_p changes markedly whilst ρ remains relatively unchanged at mode penetration is supported by C II radiation measurements at the limiter. From Fig. 10, the C II emission (proportional to the particle flux out of the plasma N/τ_p) is almost identical in form with the H_α emission ($\propto \rho N/\tau_p$), strongly suggesting that ρ remains constant whilst τ_p varies. As the RMP is turned off and the mode spins up, it can be seen from Fig. 10 that τ_p is transiently enhanced above the pre-penetration value. The energy confinement is also enhanced during this phase (see Fig. 9). This transiently enhanced confinement during the spin-up phase (when the bulk velocity is changing rapidly) is observed in most discharges with a well conditioned torus.

In the above analysis we have not included any radial profile effects when calculating N from $\bar{n}_e$. We find, however, that this is only a weak effect. For example, if $n_e \propto \sqrt{1-r^2/a^2}$, then the values of ρ and τ_p change by only about 3% from those shown in Fig. 10.

The effects of the RMP are quite different in an 'ill conditioned' torus (i.e. a torus where the walls are strongly loaded with fuelling gas). In such discharges the density usually rises at mode penetration (see Fig. 2, where the data are taken from a typical discharge with an ill conditioned torus). Analysis shows that this rise is primarily due to an increase in the recycling coefficient to unity during penetration. In such ill conditioned discharges the transient confinement enhancement during spin-up is also generally absent. The confinement enhancement is also less likely to occur in low density (i.e. $\bar{n}_e < 10^{19}$ m^{-3})

discharges and in discharges where the penetrated phase is comparatively short (i.e. ≤ 10 ms).

In summary, the particle confinement changes caused by RMPs are strongly dependent on the torus conditioning. In a well conditioned torus the density usually falls at mode penetration owing to a degradation of the particle confinement. In an ill conditioned torus the density usually rises at penetration owing to an increase in the coefficient of recycling. In a well conditioned torus a transient enhanced confinement phase is usually observed during spin-up, when the bulk plasma velocity is changing rapidly.

3.1.9. Langmuir probe data

The edge behaviour during mode penetration has been studied using a four-pin Langmuir probe. In these experiments the RMP phase relative to the probe is slowly rotated by applying sinusoidal currents in quadrature to two orthogonal sets of saddle coils. The edge electron temperature and density show a strong modulation with the RMP phase, irrespective of whether or not mode penetration has occurred. This modulation is interpreted as being due to an RMP induced change in the shape of the edge flux surface, which gives rise to an effective movement of the probe across the scrape-off layer as the RMP is rotated. The calculated flux surface distortions due to the locally non-resonant RMP (about 5 mm peak-to-peak) and the experimental scrape-off layer width are consistent with the observed temperature and density modulations with the RMP phase.

3.2. Mode unlocking

3.2.1. Introduction

In all those non-disruptive discharges in which mode penetration occurs, there is an associated 'spin-up' event soon after the RMP field is switched off. This event is clearly evident on the $m = 2$ Mirnov coil combination and the $n = 1$ locked mode traces in Fig. 2 (at $t \sim 175$ ms). Spin-up is interpreted as the island induced by the RMP field first unlocking as the electromagnetic locking torque decreases and then spinning up under the influence of the viscous torque exerted by the plasma. Simultaneously, the island decays away on a resistive time-scale since it is no longer driven by the applied RMP field.

3.2.2. Harmonic decomposition of the unlocked mode

The harmonic decomposition of the integrated $\dot{b}_\theta$ signal in geometric angle indicates that the unlocking mode is predominantly $m = 2$, with a strong $m = 3$ component ($\lesssim 40\%$ of the $m = 2$ amplitude) and a somewhat weaker $m = 1$ component ($\lesssim 30\%$ of the $m = 2$ amplitude). Transformation to a 'straight' field line angle, $\theta^* = \theta + \epsilon\lambda \sin\theta + O(\epsilon^2)$ with $\epsilon = r_M/R$ and $\lambda = 1 + l_i/2 + \beta_p$ [22], tends to reduce the amplitude of the $m = 1$ component whilst increasing that of the $m = 3$ component, but does not change our basic conclusion that the mode is predominantly $m = 2$. Taken in conjunction with the toroidal mode number measured by the small locked mode detectors (see Section 3.1.4), this result demonstrates that the penetrated mode is predominantly $m = 2$, $n = 1$.

The $m = 3$ signal is found to have a phase lag of 35–40° with respect to the $m = 2$ signal. This lag is fairly constant over a wide range of frequencies as the mode spins up. The large phase difference between the two harmonics cannot be accounted for by resistive wall effects which give a calculated phase lag of $\lesssim 4°$. One possible explanation for the difference is the presence of an $m = 3$ island in the plasma, frequency locked to the $m = 2$ island. The phases of the two islands are likely to differ because, in general, they experience different viscous torques from the plasma. The phase *lag* of the $m = 3$ island signal with respect to the $m = 2$ island signal is explicable if the accelerating viscous torque acting on the $m = 2$ island is stronger than that acting on the $m = 3$ island during spin-up. It should be noted that we observe no significant phase difference between the $m = 2$ and $m = 3$ signals for naturally unstable (2,1) modes.

The possible presence of an $m = 3$ island during spin-up is an indication that mode penetration leads to the formation of a stationary $m = 3$ island, as well as an $m = 2$ island. This is not surprising since even a pure vacuum $m = 2$ RMP field (defined in straight field line co-ordinates) will acquire an $O(\epsilon)$ $m = 3$ sideband in the presence of plasma because of toroidal coupling. The substantial reduction in bulk plasma rotation following penetration of the $m = 2$ mode is, thus, quite likely to trigger penetration of the $m = 3$ mode.

Note that the possible presence of an $m = 3$ island during the penetrated and spin-up phases is neglected, for the sake of simplicity, in the fluid models used in Sections 3.1.5 and 3.2.5 to account for the behaviour of the B IV velocity shift.

3.2.3. Measurement of the wall time constant

The fact that the spin-up event is simultaneously visible on both the Mirnov coils and the small locked mode detectors enables us to measure the wall constant of the vacuum vessel [23]. From theory, using a vacuum cyclindrical approximation for the region lying outside the mode rational surface, we expect for COMPASS-C geometry

$$H(f) = \frac{|b_\theta(r_M)|^2}{|b_R(r_L)|^2} \propto 1 + \lambda^2[1 + (r_M/r_W)^{2m}]^2$$
$$\propto 1 + 33.06(\tau_W f)^2 \tag{8}$$

where r_L is the radius of the small locked mode detectors, $r_M = 0.21$ m is the radius of the Mirnov coils, $\tau_W = \mu_0\sigma_{\text{wall}}\delta_{\text{wall}}r_W/2$ is the time constant of the wall (thickness δ_{wall}, radius $r_W = 0.22$ m, conductivity σ_{wall}), f is the mode frequency and $\lambda = 2\pi f\tau_W/m$. It follows from Eq. (8) that

$$G(f) \equiv \frac{H(f)}{f^2} = H(0)\left[\frac{1 + 33.06(\tau_W f)^2}{f^2}\right] \tag{9}$$

Figure 11 shows G_{expt} for a typical spin-up event plotted as a function of the mode frequency f. Also shown are the theoretical curves for $\tau_W = 40$, 45 and 50 μs. It can be seen that there is good agreement between theory and experiment. From Fig. 11, the best estimate for τ_W is

$$\tau_{W\,\text{expt}} \sim 45 \pm 5\ \mu\text{s} \tag{10}$$

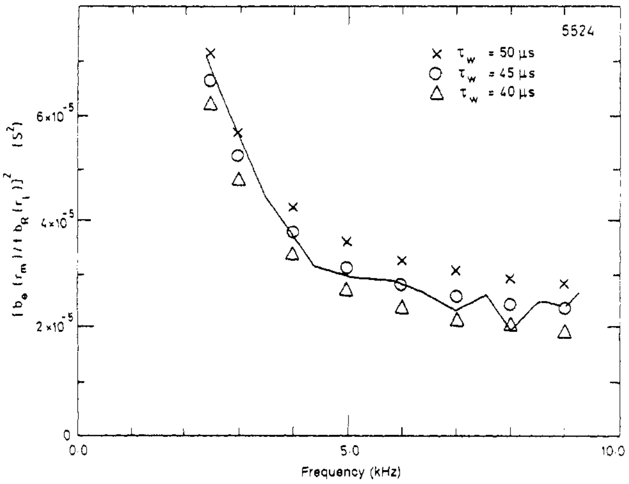

FIG. 11. Variation of the ratio $[b_\theta(r_M)/\{f b_R(r_L)\}]^2$ with frequency during the 'spin-up' of a (2,1) island. The line indicates the experimental data and the symbols show the theoretical expectation for various wall time constants (τ_W).

The above value is fairly close to the theoretical estimate for the time constant of the bellows sections of the vacuum vessel in COMPASS-C, but somewhat lower than the estimated average time constant ($\tau_W \sim 60$ μs).

3.2.4. Comparison of island decay with Rutherford island theory

According to standard Rutherford island theory [24], making use of Eq. (2), the island decay after the RMP field is switched off obeys

$$I_1\tau_R\frac{d}{dt}\left(\frac{W}{a}\right) = \Delta_0'(W)a - \frac{0.0142f^2(\text{kHz})}{1 + 0.0149f^2(\text{kHz})} \tag{11}$$

where $\tau_R = \mu_0 a^2/\eta_\parallel(r_s)$ is the resistive time-scale at the rational surface, and $I_1 = 0.822$. Using the previously mentioned vacuum cylindrical approximation and model q-profile (see Section 3.1.2), as well as the experimental value for τ_W deduced above, we obtain the following expression for the (2,1) island width as a function of the mode frequency and the $m = 2$ mode amplitude:

$$\frac{W}{a} \simeq 4\left[\frac{1}{2}\left(\frac{r_M}{a}\right)^2\left(\frac{r_M}{r_s}\right)^2\left(\frac{|b_\theta|}{r/R\,B_\phi}\right)_{r_M}\right]^{1/2}$$
$$\times \left[\frac{1 + \lambda^2\{1 - (r_s/r_W)^{2m}\}^2}{1 + \lambda^2\{1 + (r_M/r_W)^{2m}\}^2}\right]^{1/4}$$
$$= 0.072\,|b_\theta(\text{gauss})|^{1/2}\left[\frac{1 + 0.0149f^2(\text{kHz})}{1 + 0.0670f^2(\text{kHz})}\right]^{1/4} \tag{12}$$

The above expression enables us to construct $d/dt(W/a)$ from the experimental data, and thus to obtain $\Delta_0'(W)a$ as a function of τ_R from Eq. (11). Values of $\Delta_0'(W)a$ for the initial saturated rotating island width, and for the penetrated island width, have already been deduced in Section 3.1.4 for a particular discharge. Figure 12 shows $\Delta_0'(W)a$ versus W, demonstrating that the spin-up data (obtained from the same discharge) fit the assumed offset linear form (Eq. (3)) to a fairly good approximation, provided $\tau_R \simeq 45$ ms. This value of the local resistive time-scale corresponds to $T_e \sim 300$ eV at $q = 2$ (assuming neoclassical resistivity and $Z_{\text{eff}} = 2$).

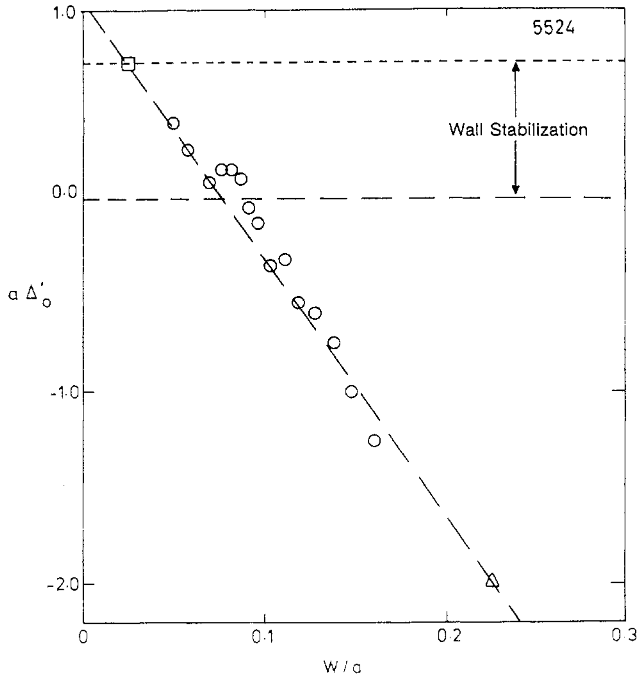

FIG. 12. Inferred variation of $\Delta_0'a$ with island width during the spin-up of a (2,1) island, calculated assuming a local resistive time-scale of 45 ms. The □ data point is deduced from the saturated amplitude of the unperturbed rotating mode, and the △ data point is deduced from the amplitude of the static penetrated mode. The curve is the fit given by Eq. (3).

Simple theoretical calculations of $\Delta'(W)$ [25] predict offset linear behaviour, but generally exhibit a somewhat steeper reduction in Δ' with increasing island width than is evident in Fig. 12. One possible explanation for this apparent discrepancy is the failure to take into account self-consistent modifications to the equilibrium due to the presence of an island. If such modifications are included in the theoretical model, a shallower $\Delta'(W)$ curve, which actually starts to increase with W beyond a certain critical island width, can be obtained [26].

3.2.5. *Analysis of island spin-up*

The decay of the velocity shift profile (Eq. (6)) during spin-up can be accounted for using the single-fluid model described in Section 3.1.5. Exponentially decaying eigenfunctions of Eq. (4) which satisfy the boundary conditions (with no discontinuities at the rational surface since there is no electromagnetic torque acting on the island after the RMP is switched off and the island inertia is neglected) take the form

$$\Delta\Omega_\phi \propto J_0(j_{0,i}\, r/a)\exp(-j_{0,i}^2\, t/\tau_\nu) \tag{13}$$

where the $j_{0,i}$ are the zeros of the Bessel function J_0, and $\tau_\nu = a^2/\nu_\perp$. Here, ρ and $\nu_\perp$ are assumed to be constant across the plasma cross-section for the sake of simplicity. It is clear that during spin-up the perturbed velocity profile will rapidly collapse to the lowest order eigenfunction, which decays at the slowest rate. Thus, our fluid model predicts a time variation of the island frequency during spin-up of the form

$$\Delta f = f_s - f \propto \exp(-t/\tau_M) \tag{14}$$

where the momentum confinement time-scale $\tau_M = \tau_\nu/5.78$ (since $j_{0,1} = 2.405$).

Figure 13 shows ln Δf plotted as a function of time during spin-up in the discharge studied in Section 3.2.4. The plot is a straight line to a good approximation, showing that Eq. (14) models the experimental data rather well. From Fig. 13, the best estimate for the momentum confinement time-scale in this discharge is $\tau_M \simeq 3.8$ ms ($\tau_\nu \simeq 22$ ms). The momentum confinement time-scale is comparable with the observed energy and particle confinement time-scales of about 4 ms, in agreement with previously reported results from TOKOLOSHE [27].

In some discharges the island initially appears to be spinning up to a frequency which is up to 2 kHz less than the pre-penetrated natural frequency f_s. We interpret this as being due to a reduction in f_s during the penetrated phase, brought about by equilibrium profile modifications.

We have examined how the momentum confinement time-scale varies for a range of discharges. At constant edge-q, we observe a very clear correlation between the local resistive time-scale τ_R, deduced from the

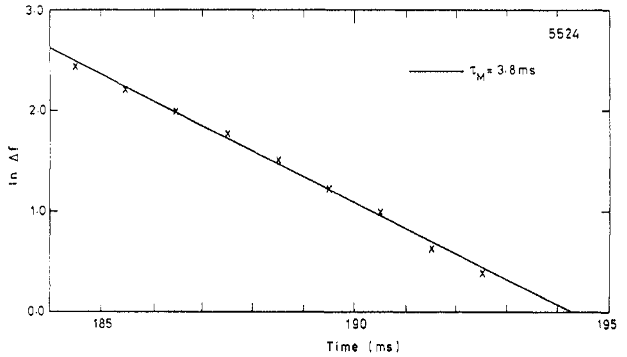

FIG. 13. Variation of the logarithm of mode frequency shift (with respect to the natural frequency) with time during mode spin-up. The curve is the fit given by Eq. (14) when τ_M = 3.8 ms.

rate of island decay, and the viscosity time-scale τ_v, deduced from the rate of island spin-up. The discharge studied in Section 3.2.5, with $\tau_R \simeq 45$ ms (corresponding to $T_e(q=2) \sim 300$ eV) and $\tau_v \sim 22$ ms, is typical of discharges which exhibit a strong confinement enhancement during the spin-up phase (see Section 3.1.8). For similar discharges in which the confinement enhancement is absent (e.g. because the torus is ill conditioned) the deduced time-scales are significantly shorter. Typical values are $\tau_R \simeq 22$ ms (corresponding to $T_e(q=2) \sim 200$ eV) and $\tau_v \simeq 12$ ms. We conjecture that the longer time-scales in the former case are characteristic of the transient enhanced confinement phase during spin-up, whereas the shorter time-scales in the latter case are characteristic of the unenhanced plasma confinement.

At constant edge-q there is a correlation between high plasma density and high τ_v. It is unclear whether this is due to increasing ease of access to the enhanced confinement phase during spin-up at higher densities or to a genuine increase in the unenhanced τ_v with plasma density. Both explanations are consistent with the data. The fact that the correlation of τ_v with τ_R is stronger than the correlation with plasma density tends to favour the former explanation.

If the decay of the velocity shift profile is dominated by a single eigenfunction, then the island frequency shift should be proportional to the spectroscopic B IV velocity shift during spin-up. For the discharge studied in Section 3.1.5 we expect

$$\frac{\Delta\Omega_\phi(r_{\mathrm{B\,IV}},t)}{\Delta\Omega_\phi(r_s,t)} = \frac{J_0(2.405\,r_{\mathrm{B\,IV}}/a)}{J_0(2.405\,r_s/a)} = 0.53 \qquad (15)$$

where $r_s = 0.67a$ is the radius of the rational surface for the model profile $q = q_\psi(r/a)^2$, $r_{\mathrm{BIV}} = 0.82a$ is the radius of the shell of radiating B IV ions (see Section 3.1.5), and $\Delta\Omega_\phi(r_s,t) = \Delta f/n$. Experimentally, the temporal behaviours of the island frequency shift and the B IV velocity shift during spin-up are indeed found to be virtually identical over a wide range of frequencies. The ratio of $\Delta\Omega_\phi(r_{\mathrm{BIV}},t)$ to $\Delta\Omega_\phi(r_s,t)$ is found to be 0.52 ± 0.02 in the discharge under consideration, which agrees well with Eq. (15). This agreement supports the argument given in Section 3.1.5 that the discrepancy between the B IV frequency shift and the mode frequency shift is dominantly due to shear in the velocity shift profile.

3.2.6. Hysteresis in the penetration/unlocking process

In Fig. 2, the spin-up event does not occur until the RMP field strength has decayed substantially below the level required to induce mode penetration. In discharges where the RMP is ramped down slowly, so that the induced stationary island remains in equilibrium with the applied RMP field, unlocking occurs somewhat earlier at about half the critical RMP field strength required for penetration. These effects are explicable in terms of our phenomenological model of mode penetration (see Appendix A). The threshold for mode penetration is calculated assuming a toroidal velocity shift scalelength of the order of the induced island width, whereas the appropriate velocity shift scalelength for the unlocking process is of the order of the minor radius (see Sections 3.1.5 and 3.2.5). This implies a far greater viscous torque acting on the induced island in the former case. Simple force balance arguments suggest that

$$\frac{I_{c\,\mathrm{unlck}}}{I_{c\,\mathrm{pntrt}}} \sim \left(\frac{W}{a}\right)_{\mathrm{pntrt}} \sim 0.23 \qquad (16)$$

(see Section 3.1.4) for the fast rampdown case and

$$\frac{I_{c\,\mathrm{unlck}}}{I_{c\,\mathrm{pntrt}}} \sim \sqrt{\left(\frac{W}{a}\right)_{\mathrm{pntrt}}} \sim 0.48 \qquad (17)$$

for the slow rampdown case. Here, we have made use of the fact that for a stationary island the ratio of the electromagnetic locking torque to the opposing viscous torque scales like $I_c W^2 l_v$, where l_v is the toroidal velocity shift scalelength. We assume that this ratio is essentially the same at mode penetration and at unlocking. For the fast rampdown case the induced island width at unlocking is assumed to be the same as that at penetration. For the slow rampdown case the induced island width is proportional to $\sqrt{I_c}$. The predictions from Eqs (16) and (17) are broadly in line with the experimental observations discussed above.

3.3. Mode stabilization

The RMP induced stabilization of rotating MHD modes observed in COMPASS-C is different in nature in low and high density discharges.

In low density ($\bar{n}_e \lesssim 10^{19}$ m^{-3}) discharges with $2 \lesssim q_\psi \lesssim 3$, the natural (2,1) mode (with a frequency of the order of 12 kHz and saturated island widths in the range $W_s/a \sim 4$–8%) decays into the noise as soon as the RMP field is applied. Results from several similar discharges ($q_\psi \sim 2.7$) are summarized in Fig. 14(a), where the $m=2$ mode amplitude is plotted against the saddle coil current (a saddle current of $I_c = 1$ kA corresponds to $b_{r(2,1)\mathrm{vac}} \sim 7$ G at the limiter for the non-helical (2,1) RMP configuration employed

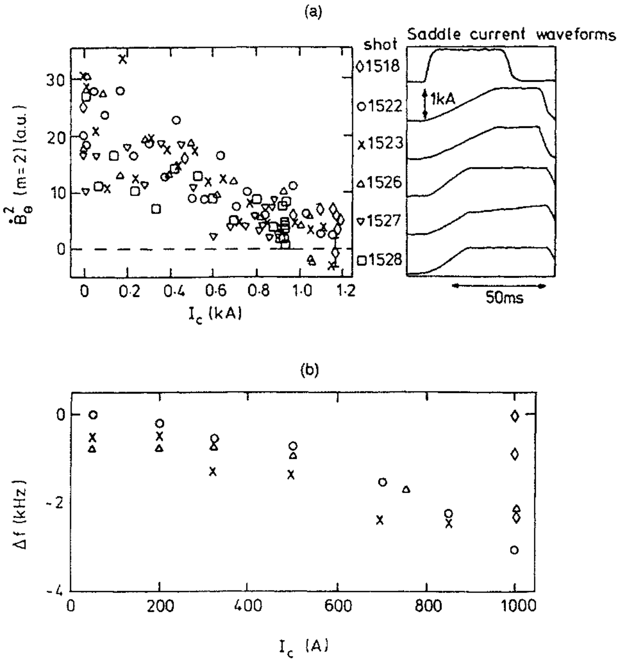

FIG. 14. (a) Reduction of the m = 2 coherent mode amplitude ($\dot{B}_\theta^2$), and (b) mode frequency shift (relative to that before the RMP is applied), with increasing (2,1) saddle current, illustrating typical 'low density' RMP mode stabilization.

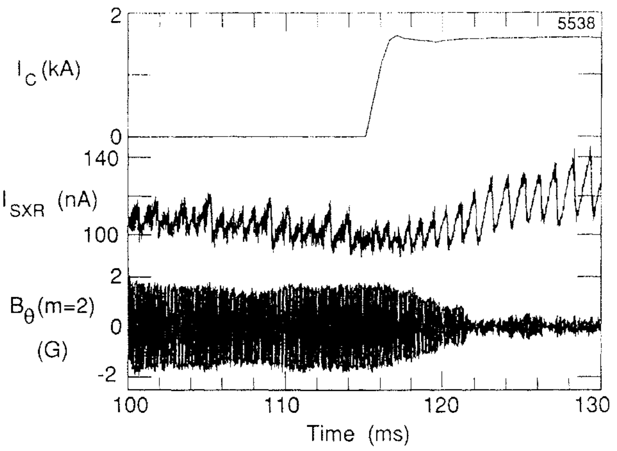

FIG. 15. Reduction in the m = 2 mode amplitude ($\dot{B}_\theta(m=2)$) upon application of a (2,1) RMP to a large (about 3.5 G) rotating natural mode, illustrating typical 'high density' RMP mode stabilization.

in this study). There is an associated frequency reduction of about 2 kHz as the (2,1) RMP field stabilizes the mode. The $m = 2$ mode frequency versus the saddle current is shown in Fig. 14(b). It can be seen that for the 'top hat' saddle current (shot 1518) the frequency reduction at $I_c = 1$ kA is not immediate (the decreasing frequency points are in chronological order at 5 ms time intervals). An analysis of a sequence of 'top hat' saddle current discharges suggests that the reduction in mode amplitude correlates with a reduction in mode frequency but not with the magnitude of the saddle current. It should be noted that this stabilization effect occurs for applied RMP fields strengths well below the mode penetration threshold, so there is a real reduction in the (2,1) island width.

Mode stabilization has also been observed at somewhat higher density ($\bar{n}_e \gtrsim 2 \times 10^{19}$ m^{-3}). In the post-boronized machine, operating in this density regime occasionally resulted in unusually large (2,1) modes ($W_s/a \sim 12\%$) becoming naturally unstable. As illustrated in Fig. 15, application of a (2,1) helical RMP field ($b_{r(2,1)\mathrm{vac}} \sim 8$ G, $b_\theta/B_\theta \sim 3.5 \times 10^{-3}$, at the limiter) results in significant stabilization of such modes over a time-scale of about 4 ms. Unlike the low density regime, this mode stabilization is not correlated with any reduction in the mode frequency, and in some cases is actually accompanied by a slight frequency *increase*. The central SXR chord in Fig. 15 indicates a slightly modified core confinement when the RMP field is switched on, although there is no evidence of any overall confinement improvement from the diamagnetic loop signal. The density rises continuously during the period when the RMP is applied, and the H_α channel indicates a change in the edge recycling. It should be noted that the regime in which these large (2,1) modes occur is not robust, in the sense that 'spontaneous' reductions in the mode amplitude are sometimes observed, and also that the mode does not generally reappear when the RMP is switched off.

In Appendix B we outline an MHD based model for the stabilization of rotating magnetic islands by static RMPs. The model predicts that mode stabilization is associated with a downward shift of the mode frequency. This stabilization mechanism is only effective for relatively low amplitude modes. For typical COMPASS-C parameters ($f_s \sim 14$ kHz, $\tau_H \sim 10^{-7}$ s, with poloidal flow damping) the critical saturated island width above which the MHD based stabilization mechanism becomes ineffective is $(W_s/a)_{\mathrm{crit}} \sim 12\%$ (see Eq. (B.3)). We propose that the RMP induced mode stabilization in low density COMPASS-C discharges is explicable in terms of this MHD based model. The most compelling evidence supporting this interpretation is the strong correlation observed between mode stabilization and a reduction in the mode frequency. According to Eq. (B.2), the observed downward frequency shift of about 2 kHz is sufficient to stabilize the relatively small rotating magnetic island encountered in the low density regime.

RMP induced mode stabilization can also be explained in terms of transport induced resistive profile evolution. According to this explanation, the changes in edge recycling and transport induced by the RMP modify the plasma equilibrium, in the process converting an otherwise unstable mode into a stable one. No particular correlation is expected between mode stabilization and a shift in the mode frequency. However, we do expect a delay, related to the energy confinement time and the resistive current profile evolution time, between the initiation of the RMP field and the stabilization of the rotating mode. The experimental data suggest that the RMP induced mode stabilization observed in high density COMPASS-C discharges is due to this type of effect. The evidence for this is the lack of any correlation between stabilization and a downward frequency shift of the mode, the time delay of about 4 ms (note that $\tau_{E\mathrm{dia}} \sim 4$ ms in COMPASS-C for the discharges under consideration) between the switching on of the RMP field and the decay of the rotating mode, and the observed changes in core energy confinement, particle confinement and edge recycling associated with the RMP.

3.4. Stimulated disruptions

It can be seen from Fig. 4 that the application of a sufficiently large RMP coil current stimulates a disruption. A typical stimulated disruption is shown in Fig. 16 for a discharge with $\bar{n}_e \simeq 1.7 \times 10^{19}$ m^{-3} and $q_\psi \sim 4.5$. Mode penetration occurs at $t \sim 118$ ms, but the disruption does not begin until $t \sim 137$ ms. No extended precursor MHD activity, such as that which normally precedes a density limit disruption, is evident before the stimulated disruption.

The observed variation of the stimulated disruption threshold with q_ψ can be modelled by assuming that the disruption is triggered when the ratio of the induced island width to the distance between the $q = 2$ radius and the limiter reaches a critical value given by $W/(a - r_s) \simeq 0.70$. This empirical disruption threshold, calculated assuming vacuum behaviour of tearing eigenfunctions external to the rational surface and a vacuum q-profile, is shown in Fig. 4. It can be seen to be in fairly good agreement with the data, except when the disruption threshold is predicted to lie below the penetration threshold. The data shown in Fig. 4 suggest that under these circumstances the disruption threshold becomes identical with the penetration threshold, indicating that the production of a large stationary island is a prerequisite for this type of disruption.

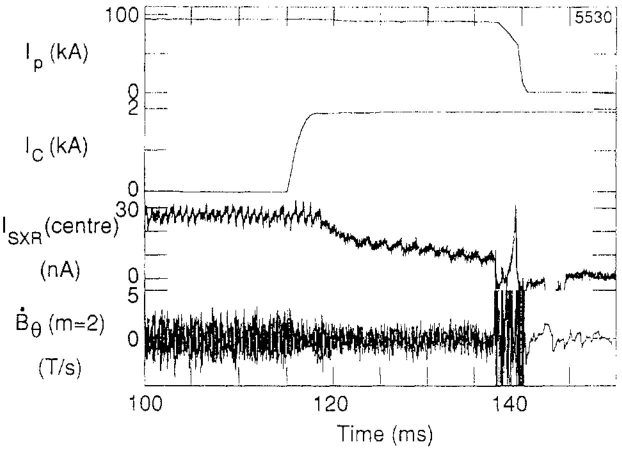

FIG. 16. Typical stimulated disruption caused by application of a large (2,1) RMP. Note that mode penetration occurs at t = 118 ms, but that the disruption does not occur until t = 137 ms. The SXR 'oscillations' following mode penetration are not believed to be sawteeth.

It is clear from the form of our empirical disruption threshold that contact between the $m = 2$ island and the limiter is not the trigger mechanism for stimulated disruptions, but the actual mechanism (e.g. contact between the induced (2,1) and (3,1) islands) has not been positively identified.

As q_ψ is reduced at fixed plasma density, we observe a gradual change in the nature of stimulated disruptions, from soft disruptions at higher edge-q, which only reduce the plasma current by about 10%, to major (or hard) disruptions at lower edge-q, which result in a complete current quench. (N.B. These results relate to RMP currents which are just sufficient to cause stimulated disruptions.) The edge-q where the transition from soft to hard disruptions occurs increases with density. For the discharges studied in Fig. 4 ($\bar{n}_e \simeq 1.25 \times 10^{19}$ m^{-3}) the transition from soft to hard disruptions appears to be coincident with the cross-over point of our empirical disruption threshold and the mode penetration threshold. At fixed edge-q, increasingly hard disruptions occur as the applied RMP field is suddenly raised further and further above the disruption threshold. We conjecture that stimulated hard disruptions occur in COMPASS-C RMP experiments when the edge-q and density are such as to cause the plasma rotation to suppress the formation of stationary islands until their size, when they appear, significantly exceeds the disruption threshold.

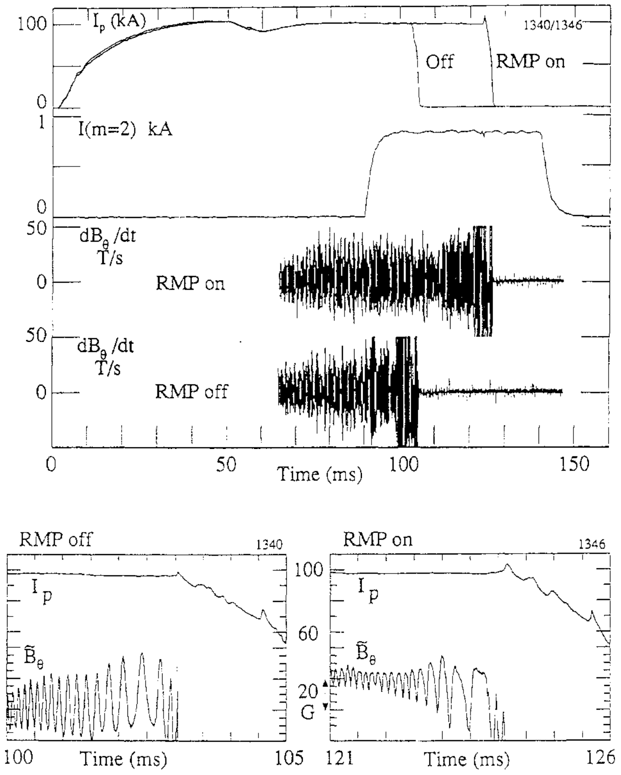

FIG. 17. Extension to the density limit disruption threshold due to the application of a (2,1) RMP, illustrated by a comparison of two 'identical' discharges, one with an $m = 2$, $n = 1$ RMP applied, and one without an RMP applied.

3.5. RMP effects on density limit disruptions

Studies of the effect of RMP fields on the density limit have been performed using (1,1), (2,1), (3,2) and (4,2) perturbations. Part-way through these experiments the wall conditions were altered by the introduction of a boronized layer. In the pre-boronization experiments, (2,1) RMP fields were observed to produce a marked increase in the density limit for $3 \leq q_\psi \leq 4.5$, whereas (1,1) and (3,2) RMP fields had no observable effect. After boronization, anomalously large (2,1) modes occasionally occurred in discharges which were far from the normal density limit (Fig. 15 shows a typical example), giving rise to premature disruptive behaviour. In such discharges, application of (3,2) RMP fields permitted non-disruptive operation at slightly higher densities.

Figure 17 presents two contrasting pre-boronization density limit discharges ($q_\psi \sim 4.3$), one with and one without an applied (2,1) RMP field. The two discharges are otherwise identical. It can be seen that the application of the RMP prolongs the discharge, permitting a higher line averaged density ($\bar{n}_e \simeq 5.2 \times 10^{19}$ m^{-3}) than would otherwise be the case ($\bar{n}_e \simeq 4.4 \times 10^{19}$ m^{-3}). It can also be seen that the $m = 2$ activity is not affected by the RMP field, except just before the disruption, where the strong asymmetric distortions to the $\dot{b}_\theta$ wave form are the expected result of the electromagnetic locking torque acting between the applied RMP field and the large natural island ($W_s/a \sim 20\%$). At the disruption, the final instability growth is enhanced in the presence of an RMP field — an effect which may be related to the larger free energy available following the temporary suppression of the disruption. With the RMP switched on, there are some indications of a change in the edge recycling (see Section 3.1.8). For instance, there is an increased rate of rise of $\bar{n}_e$ for the same gas feed rate and an increase in the H$_\alpha$ emission. Since edge recycling is known to be closely linked with the density limit [28], we conjecture that the change in edge recycling is responsible for the improved density limit. The exact mechanism by which the RMP changes the edge recycling is not clear. An RMP induced kink distortion to the outer flux surfaces (see Section 3.1.9) could perhaps alter the limiter interaction with the plasma. Alternatively, moderate to high mode number components of the RMP field resonant close to the edge of the plasma could penetrate and form stationary islands. It should be noted in this context that the probable loss of the poloidal flow damping enhancement to the mode penetration threshold (see Section A.4), due to the comparatively low ion temperatures close to the edge of the plasma, could significantly reduce the threshold.

3.6. Effect of non-(2,1) RMP configurations

We have studied the effect of applying RMPs with dominant harmonics other than $m = 2$, $n = 1$ on MHD activity.

The (3,2) RMP configuration induces mode penetration in much the same manner as the (2,1) configuration, but typically only at perturbed edge field levels two to three times the critical (2,1) level. This is explicable partly as a range effect (because $q = 3/2$ is further away from the plasma edge than $q = 2$, and the $m = 3$ perturbation decays more rapidly with radius than the $m = 2$ perturbation), and partly as a manifestation of the greater intrinsic stability of the (3,2) mode compared to the (2,1) mode (because $\Delta'_{(3,2)} < \Delta'_{(2,1)}$, see Eq. (A.29)). The occasional generation of slowly rotating (about 1 kHz) (2,1) islands following (3,2) mode penetration constitutes indirect

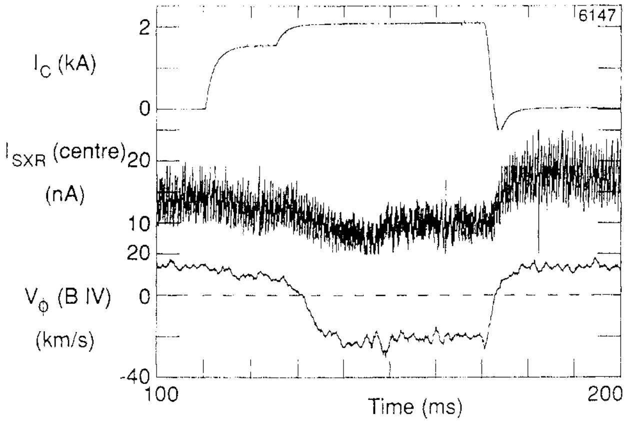

FIG. 18. Mode penetration data due to application of a predominantly (3,2) RMP. The SXR data indicate only a weak change in central confinement during mode penetration, but there is a marked change in the impurity ion toroidal velocity.

evidence for RMP induced current profile changes affecting plasma stability.

A typical (3,2) RMP discharge is shown in Fig. 18 (I_p = 95 kA, B_Φ = 0.75 T, $q_\psi \sim 3$). It is observed that sawteeth are not suppressed by (3,2) RMP fields and also that there is only a relatively small change in energy confinement following (3,2) mode penetration. As the RMP current is turned off, a rapidly decaying $m = 3$ mode is occasionally observed spinning up. The fast decay of externally induced (3,2) islands during spin-up compared to (2,1) islands is probably again due to the greater intrinsic stability of $n = 2$ modes with respect to $n = 1$ modes. Results for predominantly (4,2) RMP configurations are broadly similar to those for (3,2) configurations.

The application of a (1,1) RMP was found to have no observable effect on the sawtooth oscillation. At high (1,1) perturbation levels (up to three times those required for (2,1) mode penetration), disruptions were stimulated for $q_\psi \lesssim 3$. These disruptions, induced by the (1,1) RMP, occur at perturbed field levels close to the estimated stimulated disruption threshold for the $m = 2$ toroidally coupled sideband of the $m = 1$ RMP. We conjecture that the disruptions stimulated by the (1,1) RMP are actually due to the interaction of the (2,1) toroidally coupled sideband with the plasma. Since these (1,1) RMP results are for $q_\psi \lesssim 3$, we would expect (as is observed) that mode penetration leads directly to a stimulated disruption (see Fig. 4).

As discussed in Section 3.1.6, the $m = 1$ mode in tokamaks is special because it generally lies close to the ideal marginal stability threshold (i.e. $1/\Delta_0' a \to 0$), and its stability is not directly related to the tearing stability parameter Δ_0'. Equation (A.4) implies that, under such circumstances, only a negligible amount of reconnection can be driven at the $q = 1$ surface via an external (1,1) RMP. This in turn implies that virtually no electromagnetic torque can be generated at the $q = 1$ surface by the RMP field. Hence, the observed absence of any *direct* interaction of the (1,1) RMP with the plasma is not particularly surprising.

4. SUMMARY AND DISCUSSION

Experimental results from the COMPASS-C tokamak using externally applied static RMP fields reveal a sharp threshold field strength above which large stationary magnetic islands are induced. The sudden appearance of these islands is termed 'mode penetration'. At penetration, for an $m = 2$, $n = 1$ RMP, there is generally a strong confinement degradation, a suppression of sawteeth and a large change in the impurity ion toroidal rotation velocity.

Our observations are consistent with a phenomenological MHD model, outlined in Appendix A, which predicts that a *rotating* plasma will resist externally induced magnetic tearing until the applied RMP field strength exceeds a critical threshold. The model threshold is based on the requirements of force balance for a state in which only the plasma velocity in the immediate vicinity of the induced island is initially modified. The model does not address the dynamics of mode penetration; however, an enhanced model which deals with this area is currently under development [9]. A model for the plasma flow dynamics has also been developed which accounts for the existence of hysteresis in the penetration/unlocking process (see Section 3.2.6), and the behaviour of the impurity ion toroidal velocity during both the penetrated and spin-up phases (see Sections 3.1.5 and 3.2.5).

Mode penetration has also been observed for applied $n = 2$ ($m = 3$ and 4) RMPs (see Section 3.6). However, compared to the (2,1) RMP results, there is a far smaller degradation in confinement and little effect on sawteeth during the penetrated phase.

In all non-disruptive discharges in which mode penetration occurs, there is an associated spin-up event as the RMP is switched off. This event is interpreted as follows. The induced island first unlocks from the RMP field, as the electromagnetic locking torque becomes insufficient to balance the viscous torque acting on the island owing to the plasma, and then spins up under the influence of the latter torque. Simultaneously, the island decays away on a resistive time-scale, since it is no longer driven by the RMP field. The form of the island decay following unlocking is consistent with an offset linear variation of the intrinsic tearing stability index Δ_0' with island width. The rate of island decay enables the local resistive time-scale to be estimated (see Section 3.2.4). The momentum confinement time-scale may be estimated from the rate of island spin-up (see Section 3.2.5).

In many discharges, application of a (2,1) RMP field, which is well below that required for penetration, leads to stabilization of the natural rotating $m = 2$, $n = 1$ mode. The interpretation of this effect falls into two categories. At low density ($\bar{n}_e \lesssim 10^{19}$ m^{-3}) the mode stabilization is well correlated with a frequency reduction of about 2 kHz. This frequency reduction arises from the electromagnetic locking torque acting on the island. As discussed in Appendix B, the shear in the perturbed velocity field associated with the frequency shift has a stabilizing effect on the mode. At higher densities ($\bar{n}_e \gtrsim 2 \times 10^{19}$ m^{-3}), large amplitude rotating $m = 2$, $n = 1$ modes occasionally occur. Such modes are stabilized by application of a (2,1) RMP, but there is no correlation with any change in the mode frequency. In fact, in these cases the natural $m = 2$ islands are usually too large for the MHD based mechanism discussed in Appendix B to be effective. Instead, the stabilization is interpreted as arising from transport induced modifications to the current profile (see Section 3.3).

Application of (2,1) RMP fields has been used both to stimulate and to control disruptions. A scan of the edge-q at constant density suggests that the production of a large stationary island is a necessary (but not sufficient) condition for a stimulated disruption to occur (see Section 3.4). Control of natural density limit disruptions, with an approximately 15% increase in the $\bar{n}_e$ limit, was observed when (2,1) RMP fields were applied to pre-boronized discharges with $3 \lesssim q_\psi \lesssim 4.5$. In these cases, the improved density limit is interpreted as a manifestation of the RMP induced change in the edge recycling behaviour, possibly caused by the production of moderate to high mode number islands close to the edge of the plasma or by a kink distortion to the outermost flux surfaces.

The perturbed edge field levels required to induce mode penetration in COMPASS-C are extremely high ($b_{r(2,1)}/B_\phi \gtrsim 10^{-3}$) owing to the comparatively small dimensions of the device and the associated high MHD mode rotation frequencies ($f_s \gtrsim 10$ kHz). In larger devices (e.g. DIII-D, JET) the threshold perturbation level predicted by our model is much smaller (e.g. $b_{r(2,1)}/B_\phi \sim 10^{-4}$). In fact, in such devices error fields will play a role analogous to that of the deliberately applied RMP fields in COMPASS-C. Error field induced locked modes would manifest themselves as essentially *precursorless* locked modes growing on a *resistive evolution time-scale*. The appearance of such modes should be strongly correlated with *low plasma density* and *low edge-q*. Such modes are indeed observed on DIII-D and JET [29, 30], at approximately the error field levels predicted by our model.

In summary, many of the seemingly diverse effects observed in the COMPASS-C RMP experiments and in previous experiments can be explained in terms of a phenomenological model which combines standard tearing mode electromagnetic theory with a viscous single-fluid treatment of the plasma (see Appendix A). This model allows the effects of error fields in future large tokamaks (e.g. ITER [31]) to be assessed. For example, for ITER parameters (assuming $B_\phi = 4.9$ T, $I_p = 17$ MA) we find a very low penetration threshold (assuming Ohmic mode rotation) of $b_{r(2,1)}/B_\phi \sim 2 \times 10^{-5}$. This indicates that the limitation to the disruption free operating space due to the formation of locked modes at low density observed in DIII-D [29] is also likely to occur in ITER. It should be noted, however, that if the natural mode frequency is artificially increased (e.g. by the application of unbalanced neutral beam heating), then the error field penetration threshold is also likely to be increased.

Appendix A

A PHENOMENOLOGICAL MODEL OF MODE PENETRATION

A.1. Preamble

In this appendix we describe a phenomenological model of the penetration of a static RMP into a rotating tokamak plasma. Mode penetration is most easily dealt with in cylindrical geometry. With the exception of poloidal flow damping, which can have a profound influence on the penetration threshold, toroidicity does not introduce significant additional physics into the problem. Later on (in Section A.4) we shall describe how poloidal flow damping can be introduced into our cylindrical model.

A.2. Magnetic reconnection driven by external RMPs

Consider a tearing stable, cylindrical plasma equilibrium. Suppose that a static (m, n) RMP, resonant at

r_s inside the plasma, is applied via helical field windings external to the plasma. The perturbed magnetic field is written $\mathbf{b} = \nabla\psi\times\hat{\mathbf{z}}$, where $\psi = \psi(r)\, e^{i(m\theta - n\phi)}$ is the perturbed flux, satisfying the conventional cylindrical tearing mode equation [32]. Here, θ and ϕ are the poloidal and (simulated) toroidal angles, m and n are the poloidal and toroidal mode numbers, and $\hat{\mathbf{z}}$ is the unit symmetry axis in cylindrical geometry. The simulated toroidal angle is defined as $\phi = z/R$, where z is the distance along the $\hat{\mathbf{z}}$ axis and R is the simulated major radius.

It is convenient to split the perturbed flux eigenfunction $\psi(r)$ into two separate components. The first component, ψ_1, is the RMP eigenfunction in the presence of a plasma which satisfies the *ideal* MHD constraint ($\psi(r_s) = 0$). Note that $\psi_1(r < r_s) = 0$, since the mode rational surface acts like a perfectly conducting wall in an ideal plasma. The function ψ_1 typically reaches a steady state in the time required for a shear Alfvén wave to traverse the discharge (10^{-7} s for most tokamaks) [33]. Thus, for the purposes of our discussion, ψ_1 is set up 'instantaneously' as soon as the helical field windings are energized. In general, ψ_1' ($' \equiv \partial/\partial r$) is discontinuous at r_s, implying the existence of a helical current sheet on the rational surface. Finite island modifications to the RMP eigenfunction ψ_1 are not as significant as those to the natural eigenfunction ψ_0 and are therefore neglected in the following.

The second component, ψ_0, is the familiar tearing mode eigenfunction, matched to vacuum boundary conditions at the plasma edge. In general, $\psi_0(r_s) \equiv \Psi$ is non-zero, implying the presence of an island of width

$$W = 4\left(\frac{Rq_s}{B_\phi}\frac{\Psi}{s}\right)^{1/2} \tag{A.1}$$

at the mode rational surface. Here, B_ϕ is the toroidal field strength, $s = (rq'/q)_{r_s}$ is the magnetic shear at the rational surface, $q(r)$ is the usual safety factor and $q_s = q(r_s)$. Using the standard approximation, we assume that ψ_0 is constant across the island region, but that ψ_0' is discontinuous at $r_{s\pm} = r_s \pm W/2$, again implying the existence of helical current sheets in the vicinity of the rational surface. It is convenient to parametrize these sheet currents by the quantity

$$\Delta_0'(W) = \frac{[\psi_0']_{r_{s-}}^{r_{s+}}}{\Psi} \tag{A.2}$$

where $[\psi_0']_{r_{s-}}^{r_{s+}}$ is the net discontinuity in ψ_0' in the vicinity of the rational surface. A more generalized quantity, Δ', which parametrizes the total sheet current associated with *both* eigenfunctions, is defined as

$$\Delta'(W) = \Delta_0'(W) + \frac{\psi_1'(r_s)}{\Psi} \tag{A.3}$$

A resistive plasma will evolve towards a final steady state in which there is *zero* sheet current in the vicinity of the rational surface [24]. Such a state can be constructed by forming a linear combination of ψ_0 and ψ_1 such that $\Delta' = 0$. This implies a final reconnected flux at the rational surface

$$\Psi_0 = \frac{(\psi_1' r)_{r_s}}{[-\Delta_0'(W_0)\, r_s]} \tag{A.4}$$

with an associated island width W_0. Henceforth, we shall refer to Ψ_0 as the 'fully reconnected' flux and to W_0 as the 'fully reconnected' island width. According to standard non-linear island theory [24], the natural eigenfunction ψ_0 can only evolve on a resistive time-scale. Thus, the plasma can only attain its final, fully reconnected state at a time of the order of $(W_0/a)\tau_R$ after the RMP is switched on. Here, a is the plasma minor radius and τ_R is the time-scale for the magnetic field to diffuse a distance a.

Suppose that the plasma current is mostly concentrated inside the rational surface at r_s, so that the plasma outside the rational surface is vacuum-like (i.e. it carries zero equilibrium current). This is a reasonable approximation if the rational surface lies towards the edge of the discharge ($r/a \gtrsim 0.6$), as is usually the case in (2,1) RMP experiments. Using this assumption, we can write

$$\Psi_0 = \left(\frac{2m}{-\Delta_0'(W_0)r_s}\right)\Psi_c \tag{A.5}$$

and

$$W_0 = \left(\frac{2m}{-\Delta_0'(W_0)r_s}\right)^{1/2} W_c \tag{A.6}$$

Here, Ψ_c is the flux at the rational surface due to the *vacuum* RMP eigenfunction and W_c is the associated *vacuum* island width. Note that the ratio of fully reconnected to vacuum island widths is unity when $\Delta_0'(W_0)r_s = -2\,m$, which is only likely to be the case if the current profile is completely relaxed (i.e. $j' = 0$) or the poloidal mode number is very high. Both these situations can be expected to be maximally stable to tearing modes. In typical tokamak discharges the non-zero current gradients inside the rational surface *destabilize* low mode number tearing modes to some extent, giving $-\Delta_0'(W_0)r_s > 2\,m$. It follows from Eqs (A.5) and

(A.6) that under these circumstances the plasma will tend to *amplify* any low mode number perturbations which penetrate into it [34, 35] (i.e. the fully reconnected island will be larger than the vacuum island). This effect becomes more pronounced as $-\Delta_0'(W_0)r_s$ becomes small. Equation (A.6) is, of course, an implicit equation for W_0 owing to the variation of Δ_0' with island width. It is easily demonstrated that a unique solution with $\Delta_0'(W_0) < 0$ always exists, provided that Δ_0' is a monotonic decreasing function of the island width.

A.3. Suppression of driven magnetic reconnection by plasma rotation

A.3.1. Introduction

It is clear from the above that the preferred response of a resistive plasma to an externally applied, *static* RMP is the formation of a fully reconnected, stationary island on a resistive time-scale. We now outline how plasma rotation can, under certain circumstances, prevent the 'penetration' of an RMP (i.e. formation of a stationary island), in effect forcing the plasma to respond *ideally* to the applied perturbation. The experimental data obtained from the COMPASS-C tokamak indicate that mode penetration is characterized by the complete absence of any rotating precursor, in marked contrast to conventional 'mode locking' [10]. Any rotating Mirnov activity which is present before the application of the RMP appears to be stabilized via the MHD mechanism (discussed in Appendix B) *before* the onset of mode penetration.

In the following, we develop a simple model of mode penetration. It turns out that there are two distinct contributions to the penetration threshold. The first is associated with plasma *viscosity* and the second with plasma *inertia*. These contributions are initially evaluated separately, but then they are combined to give a general threshold (Section A.5).

Let us suppose that mode penetration takes place in two stages. In the first stage, only the plasma velocity in the immediate vicinity of the rational surface is modified as the stationary island forms. In the second stage, the velocity profile relaxes across the whole plasma cross-section under the influence of viscosity. The effects of viscosity and inertia on the island during the first stage are far larger than those during the second stage because of the higher velocity shears in the vicinity of the rational surface, and are assumed to be the controlling factors which determine whether or not mode penetration occurs. In principle, a complete description of the first stage of mode penetration involves the solution of a very complicated dynamic problem in which the island evolves under the influence of time dependent viscous, inertial and electromagnetic forces. We propose, however, that an approximate penetration threshold can be obtained via a far less complicated approach. We suggest that the occurrence of mode penetration is solely dependent on the existence of a quasi-steady stationary island state in which only the plasma in the vicinity of the island is brought to rest (i.e. the velocity scalelength in the vicinity of the rational surface is $O(W)$). This model has the advantage that it gives rise to relatively simple expressions for the penetration threshold, and the disadvantage that it sheds no light on the *dynamics* of the first stage of mode penetration. The dynamics of mode penetration is currently under investigation [9].

A.3.2. The viscous penetration threshold

In a viscous, rotating plasma the phase shift of the induced stationary island with respect to the RMP field ($\Delta\varphi$, say) is, in general, non-zero. In the presence of a finite phase shift, the driven Rutherford island equation takes the form

$$\frac{dW}{dt} \propto [-\Delta_0'(W)r_s]\left[\left(\frac{W_0}{W}\right)^2 \cos\Delta\varphi - 1\right] \tag{A.7}$$

where the fully reconnected island width W_0 now satisfies Eq. (A.6), with $\Delta_0'(W_0) \to \Delta_0'(W)$. It follows that in a quasi-steady state

$$W = W_0\sqrt{\cos\Delta\varphi} \tag{A.8}$$

The electromagnetic locking torque which develops in the island region takes the form

$$\begin{aligned} f_{\theta\,\mathrm{EM}} &= \int_{r_{s-}}^{r_{s+}} r\delta B_r \delta j_\phi \, r\,dr \\ &\simeq \frac{r_s^2}{\mu_0}\left(\frac{B_\phi n s r_s}{16R}\right)^2 \left(\frac{W}{r_s}\right)^2 \left(\frac{W_c}{r_s}\right)^2 \sin\Delta\varphi \end{aligned} \tag{A.9}$$

where use has been made of the usual vacuum approximation outside the rational surface.

The viscous force acting on the island is evaluated using a variant of the single-fluid model outlined in Section 3.1.5. Thus, for a non-poloidally flow damped plasma the poloidal component of the single-fluid equation of angular motion is written

$$\rho\frac{\partial\Delta\Omega_\theta}{\partial t} = \frac{1}{r^3}\frac{\partial}{\partial r}\left[(\rho\nu_\perp r^3)\frac{\partial\Delta\Omega_\theta}{\partial r}\right] \qquad \text{(A.10)}$$

where $\Delta\Omega_\theta$ is the poloidal angular velocity shift. The velocity shift at the rational surface is related to the island frequency shift via

$$m\Delta\Omega_\theta(r_s) = 2\pi(f - f_s) \qquad \text{(A.11)}$$

The viscous torque acting on a stationary ($f = 0$) island during the first stage of mode penetration is given by

$$\begin{aligned} f_{\theta\nu} &= \left[(\rho\nu_\perp r^3)\frac{\partial\Delta\Omega_\theta}{\partial r}\right]_{r_{s-}}^{r_{s+}} \\ &\sim r_s^3\rho(r_s)\nu_\perp(r_s)\frac{\Delta\Omega_\theta(r_s)}{W} \end{aligned} \qquad \text{(A.12)}$$

since the velocity scalelength in the vicinity of the rational surface is O(W).

Torque balance (i.e. $f_{\theta\mathrm{EM}} + f_{\theta\nu} = 0$) plus Eqs (A.8) and (A.11) yield the following condition for the existence of a quasi-steady state during the first stage of mode penetration:

$$\begin{aligned} F &\equiv \frac{1024\pi}{(ns)^2}\left(\frac{f_s\tau_H^2}{[-\Delta_0'(W)r_s](r_s/a)^2\tau_\nu}\right)\Big/\left(\frac{W_0}{r_s}\right)^5 \\ &= (\cos\Delta\varphi)^{3/2}\sin\Delta\varphi \end{aligned} \qquad \text{(A.13)}$$

where $\tau_H = R\sqrt{\mu_0\rho(r_s)}/B_\Phi$ is the local hydromagnetic time-scale and $\tau_\nu = a^2/\nu_\perp(r_s)$ is the so-called viscosity time-scale.

The parameter F is essentially the viscous torque normalized with respect to the electromagnetic locking torque. For $F < (3/5)^{3/4}(2/5)^{1/2} = 0.431$, there are two solutions to the above equation. The first ($\Delta\varphi < \cos^{-1}\sqrt{3/5} = 39.2°$) is stable, and the second ($\Delta\varphi > 39.2°$) is unstable. As the normalized viscous torque (i.e. F) is gradually increased from zero, the stable phase shift increases monotonically from zero and the corresponding quasi-steady island width decreases monotonically from W_0 (i.e. the island 'partially reconnects'), whilst the unstable phase shift decreases monotonically from $\pi/2$. Eventually, a critical point (i.e. $F = 0.431$) is reached at which the two solutions coalesce and any further increase in F leads to a viscous torque which cannot be balanced by the electromagnetic locking torque. The driven island width $W_{\mathrm{min}} = 0.8801\,W_0$ at this point is the minimum which can be achieved in a quasi-steady state. Likewise, the phase shift $\Delta\varphi_{\mathrm{max}} = 39.2°$ is the maximum achievable one in a quasi-steady state. According to our model, the critical value of the normalized viscous torque above which it is impossible to maintain a quasi-steady state island (i.e. $F = 0.431$) is the value required to prevent mode penetration. Thus, our model *viscous* penetration criterion takes the form

$$\begin{aligned} \frac{W_0}{a} &\geq \frac{(W_0)_{\mathrm{crit}}}{a} \\ &= 5.95\frac{(r_s/a)^{2/5}}{(ns)^{2/5}}\frac{(f_s\tau_H^2/\tau_\nu)^{1/5}}{[-\Delta_0'(0.8801W_0)a]^{1/5}} \end{aligned} \qquad \text{(A.14)}$$

The above threshold has been derived under the assumption that only the plasma in the immediate vicinity of the induced island is brought to rest during the crucial first stage of penetration. The relaxation of the velocity profile during the second stage of mode penetration will tend to increase the velocity scalelength in the vicinity of the island and so reduce the viscous torque. It follows that our simple model predicts a *hysteresis* effect; i.e. once penetration has occurred and the velocity profile has had sufficient time to relax, the RMP amplitude must be reduced significantly below the critical value for penetration in order to remove the stationary island from the plasma.

A contemporaneous study of the viscous suppression of forced reconnection in rotating plasmas has reached conclusions which are consistent with the above [36].

A.3.3. The inertial penetration threshold

The influence of inertia on mode penetration is slightly more subtle than that of viscosity. Consider what happens when a stationary island is driven in a tearing stable, rotating plasma. During the crucial first stage of penetration, the velocity shift profile $\Delta\mathbf{v}$ of our phenomenological single fluid is strongly sheared in the vicinity of the island. In a quasi-steady state the advective inertia associated with this sheared velocity field, $\rho(\Delta\mathbf{v}\cdot\nabla)\Delta\mathbf{v}$, must be balanced by electromagnetic forces. This is achieved via a perturbed perpendicular polarization current of the form

$$\mathbf{j}_{p\perp} = \frac{\rho}{B^2}(\Delta\mathbf{v}\cdot\nabla)\Delta\mathbf{v}\wedge\mathbf{B} \qquad \text{(A.15)}$$

Note that we are able to write the perturbed advective inertia in terms of a phenomenological single-fluid velocity which is almost certainly not identical with the ion fluid velocity because it is only the *shear* in the perturbed ion fluid velocity which ultimately matters. As is discussed in Section 3.1.5, we assume that velocity shifts $\Delta\mathbf{v}$ in our phenomenological fluid give rise to approximately equal shifts in the ion fluid velocity, i.e. the shear in the perturbed ion fluid velocity is the same as the shear in $\Delta\mathbf{v}$.

Quasi-neutrality requires that $\nabla\cdot\mathbf{j} = 0$, so we can write

$$\nabla_{\|} j_{\|\,\mathrm{inertia}} + \nabla_{\perp}\cdot\mathbf{j}_{p\perp} = 0 \tag{A.16}$$

where $j_{\|\,\mathrm{inertia}}$ is the additional perturbed parallel current due to inertial effects. The parallel and perpendicular gradient operators can be crudely approximated as

$$\begin{aligned} \nabla_{\|} &\sim \frac{m}{r_s}\frac{s}{Rq_s}W \\ \nabla_{\perp}\cdot\mathbf{j}_{p\perp} &\sim \frac{j_{p\perp}}{W} \end{aligned} \tag{A.17}$$

since the velocity scalelength in the vicinity of the rational surface is assumed to be O(W). Equations (A.15) and (A.16) yield

$$j_{\|\,\mathrm{inertia}} \sim \frac{r_s}{m}\frac{Rq_s}{s}\frac{\rho}{B_\phi}\frac{|(\Delta\mathbf{v}\cdot\nabla)\Delta\mathbf{v}|}{W^2} \tag{A.18}$$

If the plasma flow is not strongly poloidally damped, we can write

$$|(\Delta\mathbf{v}\cdot\nabla)\Delta\mathbf{v}| \sim m r_s \Delta\Omega_\theta^2(r_s) \sim \frac{r_s}{m}(2\pi f_s)^2 \tag{A.19}$$

From the definition of Δ', from Maxwell's equations and from Eqs (A.2)–(A.4), the quasi-steady Rutherford island equation takes the form

$$\begin{aligned} \frac{dW}{dt} &\propto \Delta_0'(W)\left[1 - \left(\frac{W_0}{W}\right)^2\right] \\ &\qquad + \mu_0 \int_{r_s-}^{r_s+} j_{\|\,\mathrm{inertia}}\, dr \Big/ \Psi = 0 \end{aligned} \tag{A.20}$$

Making use of Eqs (A.18) and (A.19), and writing $\int_{r_s-}^{r_s+} j_{\|\,\mathrm{inertia}} dr \sim W j_{\|\,\mathrm{inertia}}$, the above equation reduces to

$$\begin{aligned} \frac{dW}{dt} &\propto [-\Delta_0'(W)\, r_s]\left[\left(\frac{W_0}{W}\right)^2 - 1\right] \\ &\qquad + C\frac{(\tau_H f_s)^2}{(ns)^2(W/r_s)^3} = 0 \end{aligned} \tag{A.21}$$

where C is a numerical constant. In Ref. [37] it is demonstrated that $C = -1210.4$. Thus, the inertial contribution to the Rutherford island equation is *stabilizing*.

We conclude that during the first stage of penetration the strongly sheared velocity shift profile in the vicinity of the rational surface has a stabilizing effect on the induced island, causing it to only partially reconnect (i.e. $W < W_0$). It can easily be demonstrated that there is a critical value of the inertial stabilization term in Eq. (A.21) above which no quasi-steady solutions exist, and that the final quasi-steady state is characterized by $W = 0.5774\,W_0$. In accordance with our model, we identify this critical value of the inertia as the value required to prevent mode penetration. Thus, our *inertial* penetration criterion takes the form

$$\begin{aligned} \frac{W_0}{a} &\geq \frac{(W_0)_{\mathrm{crit}}}{a} \\ &= 14.6\frac{(r_s/a)^{2/3}}{(ns)^{2/3}}\frac{(f_s\tau_H)^{2/3}}{[-\Delta_0'(0.5774W_0)a]^{1/3}} \end{aligned} \tag{A.22}$$

Previous numerical studies of the inertial suppression of forced reconnection in rotating plasmas have reached conclusions consistent with the above [38–40]. Strongly sheared flows, such as those occurring during the first stage of mode penetration, are always found to be stabilizing [38], whereas weakly sheared flows can be destabilizing [39].

A.4. Poloidal flow damping

A study of the slowing down of large rotating magnetic islands in JET due to eddy currents induced in the resistive vacuum vessel suggests that the change in plasma rotation is almost entirely *toroidal* in nature [10]. This effect is due to strong poloidal flow damping, arising in a toroidally confined plasma, which rapidly damps out any perturbed poloidal flow [41]. Although the mode penetration theory outlined above is intrinsically cylindrical, poloidal flow damping can be incorporated as follows.

There are three basic effects which must be taken into account when transforming from a freely rotating system to a poloidally damped system. Firstly, the toroidal component of the electromagnetic locking force is a factor $(r/qR)_{r_s}$ smaller than the poloidal component. Secondly, a given change in the mode frequency corresponds to a far larger (by a factor $(qR/r)_{r_s}$) change in the plasma velocity in a poloidally damped system than in a freely rotating one. Finally, in a poloidally damped system the advective inertial force acting on a stationary island during the first stage of mode penetration is of the order of

$$|(\Delta \mathbf{v} \cdot \nabla)\Delta \mathbf{v}| \sim nR\Delta\Omega_\phi^2(r_s) \sim \frac{R}{n}(2\pi f_s)^2 \tag{A.23}$$

which is a factor of $(qR/r)_{r_s}$ larger than the corresponding inertial force in a freely rotating system (see Eq. (A.19)).

A.5. Criterion for mode penetration

After some manipulation, using the previous results and the analysis of Ref. [37], our model mode penetration criterion reduces to

$$\begin{aligned} \frac{W_0}{a} &\geq \frac{(W_0)_{\rm crit}}{a} \\ &= 5.8\frac{g(\zeta)\mathcal{I}^{2/5}(r_s/a)^{2/5}}{(ns)^{2/5}}\frac{(f_s\tau_H^2/\tau_\nu)^{1/5}}{(-\Delta_0'a)^{1/5}} \end{aligned} \tag{A.24}$$

where

$$\begin{aligned} 0 &= g^5 - g^2/\zeta^3 - 1, \\ \zeta &= 0.397\left[\frac{\mathcal{I}^{1/3}(-\Delta_0'a)^{2/3}(ns)^{4/3}}{f_s^{7/3}\tau_\nu\tau_H^{4/3}(r_s/a)^{4/3}}\right]^{1/5} \end{aligned} \tag{A.25}$$

and

$$\mathcal{I} = \begin{cases} 1 & \text{for poloidal rotation} \\ (qR/r)_{r_s} & \text{for toroidal rotation} \end{cases} \tag{A.26}$$

In the limit $\zeta \ll 1$, inertial effects are dominant, whereas viscous effects are dominant in the limit $\zeta \gg 1$. For realistic tokamak plasma parameters, viscosity tends to be the more important of the two effects.

The following formulas for the critical fraction of reconnection and for the island phase shift with respect to the vacuum island during the first stage of penetration are both accurate to within a few per cent:

$$\begin{aligned} \bar{W}_{\rm min} = \frac{W_{\rm min}}{W_0} &= 0.5774\left[\frac{1+1.495\bar{\zeta}_\nu}{1+\bar{\zeta}_\nu}\right] \\ \sin\Delta\varphi_{\rm max} &= 2\left[\frac{\bar{\zeta}_\nu(1+\bar{\zeta}_\nu)^2}{(1+1.495\bar{\zeta}_\nu)^3}\right] \end{aligned} \tag{A.27}$$

where

$$\bar{\zeta}_\nu = \zeta^3 g^3(\zeta) - 1 \tag{A.28}$$

Note that inertial effects are never entirely negligible, even in the high viscosity limit, $\zeta \gg 1$, because of viscously induced circulatory flows inside the island separatrix (see Ref. [37]). This accounts for the fact that Eq. (A.24) does not quite asymptote to Eq. (A.14) in the limit $\zeta \to \infty$.

Making use of the usual vacuum cylindrical approximation for the region of the plasma lying outside the mode rational surface, Eq. (A.24) implies a critical vacuum radial RMP field strength at the edge of the plasma ($r = a$) for penetration, given by

$$\begin{aligned} \left[\frac{b_{r\,\rm vac}}{\epsilon B_\phi}\right]_a \geq \left[\frac{(b_{r\,\rm vac})_{\rm crit}}{\epsilon B_\phi}\right]_a &= \frac{1.06}{m}\left(\frac{r_s}{a}\right)^{2-m} \\ &\times\ g^2(\zeta)\mathcal{I}^{4/5}\frac{(ns)^{1/5}}{(r_s/a)^{1/5}}\left(\frac{f_s\tau_H^2}{\tau_\nu}\right)^{2/5}(-\Delta_0'a)^{3/5} \end{aligned} \tag{A.29}$$

where $\epsilon = r/R$. The expected relative increase in the perturbed edge radial field at mode penetration is

$$\left[\frac{\Delta b_r}{(b_r)_{\rm crit}}\right]_a = \left[\frac{(r_s/a)^{2m}}{1-(r_s/a)^{2m}}\right]\left(\frac{2m}{-\Delta_0' r_s}\right)\bar{W}_{\rm min}^2 \tag{A.30}$$

Note that in Eqs (A.24) to (A.30)

$$\Delta_0' \equiv \Delta_0'[W_{\rm crit}] \equiv \Delta_0'[\bar{W}_{\rm min}(W_0)_{\rm crit}] \tag{A.31}$$

If $\Delta_0'(W)$ is not constant, then Eqs (A.24)-(A.30) become implicit for $(W_0)_{\rm crit}$ and can only be solved by iterative techniques. If Δ_0' is a monotonically decreasing function of W, then it is easily demonstrated that a unique solution exists.

Appendix B

THE STABILIZATION OF ROTATING MHD ACTIVITY

The interaction of a moderate amplitude static RMP field with a saturated rotating magnetic island gives rise to two main effects. Firstly, the average rotation frequency of the island is slightly reduced and, secondly, the island rotation becomes slightly non-uniform. Both of these effects can have a stabilizing influence on the natural mode, the first because of the velocity shear associated with the frequency shift and the second because the non-uniformly rotating island actually spends slightly more time in the stabilizing phase of the RMP field than in the destabilizing phase. In the following, we outline a rather simplistic model of the velocity shear stabilization mechanism.

Analysis of Sections A.3.3 and A.4 suggests that an RMP induced island frequency shift Δf gives rise to a stabilizing term in the Rutherford island equation of the form

$$\frac{d}{dt}\left(\frac{W}{a}\right) \propto \Delta_0'(W)a - 1210.4\,\mathcal{I}\frac{(\Delta f \tau_H)^2}{(ns)^2(W/r_s)^2} \tag{B.1}$$

where it is assumed that the perturbed velocity scale-length is of the order of the minor radius owing to the effect of plasma viscosity. Equation (B.1) implies an approximate criterion for significant MHD mode stabilization, given by

$$\Delta f \gtrsim (\Delta f)_{\rm crit} \simeq \left(\frac{ns}{\tau_H}\right)\left[\frac{[-\Delta_0'(W_s)a]}{1210.4\,\mathcal{I}}\right]^{1/2}\left(\frac{W_s}{a}\right) \tag{B.2}$$

where W_s is the initial saturated island width. Now, the RMP induced frequency shift Δf is unlikely to exceed the initial mode frequency f_s. In fact, once the island is brought to rest, any further increase in the RMP field strength is likely to lead to an *increased* island width via direct driving from the RMP. It follows that for a given mode frequency f_s there is a maximum saturated island width which can be effectively stabilized. From Eq. (B.2), this critical island width is given by

$$\left(\frac{W_s}{a}\right)_{\rm crit} \sim \left[\frac{1210.4\,\mathcal{I}}{[-\Delta_0'(W_s)a]}\right]^{1/2}\left(\frac{f_s\tau_H}{ns}\right) \tag{B.3}$$

According to our model, if $W_s \ll (W_s)_{\rm crit}$, then the application of a ramped RMP field leads to mode stabilization, eventually followed by mode penetration. If $W_s \gtrsim (W_s)_{\rm crit}$, then the application of a ramped RMP field leads to conventional mode locking, with little effect on the mode amplitude. These conclusions have been confirmed by numerical resistive MHD simulations which exhibit a stabilizing effect for smaller islands and mode locking at virtually constant island amplitude for larger islands. Thus, both analytic theory and numerical simulations suggest that relatively low amplitude saturated, rotating islands can be stabilized by the application of static RMP fields. The stabilization effect is associated with a downward frequency shift of the mode.

ACKNOWLEDGEMENTS

It is a pleasure to acknowledge the invaluable contributions made by J.H. Hay and the COMPASS-C engineering team, J.R. Watkins and the operations team, and S.D. Hanks and the technical team. Thanks are also due to P. Nicholson, S.J. Manhood and K. Stammers. Two of the authors (R.F. and T.C.H.) are also indebted to J.A. Wesson for discussions on the stabilization of rotating modes.

This work was jointly funded by the United Kingdom Department of Trade and Industry and by Euratom.

REFERENCES

[1] KARGER, F., WOBIG, H., CORTI, S., et al., in Plasma Physics and Controlled Nuclear Fusion Research 1974 (Proc. 5th Int. Conf. Tokyo, 1974), Vol. 1, IAEA, Vienna (1975) 207.

[2] ELLIS, J.J., HOWLING, A.A., MORRIS, A.W., ROBINSON, D.C., in Plasma Physics and Controlled Nuclear Fusion Research 1984 (Proc. 10th Int. Conf. London, 1984), Vol. 1, IAEA, Vienna (1985) 363.

[3] ROBERTS, D.E., SHERWELL, D., FLETCHER, J.D., NOTHNAGEL, G., De VILLIERS, J.A.M., Nucl. Fusion **31** (1991) 319.

[4] HAYWARD, R.J., CRAWLEY, P.J., CROSSLAND, R.T., INGRAM, B.S., PRATT, A.P., SMITH, R.T.C., in Fusion Technology (Proc. 15th Symp. Utrecht, 1988), Vol. 1, North-Holland, Amsterdam (1988) 361.

[5] MORRIS, A.W., CAROLAN, P.G., FITZPATRICK, R., HENDER, T.C., TODD, T.N., Phys. Fluids B **4** (1992) 413.

[6] FIELDING, S.J., AXON, K.B., CAROLAN, P.G., et al., in Controlled Fusion and Plasma Physics (Proc. 18th Eur. Conf. Berlin, 1991), Vol. 15C, Part III, European Physical Society (1991) 73.

[7] La HAYE, R.J., SCOVILLE, J.T., Rev. Sci. Instrum. **62** (1991) 2146.

[8] CROSSLAND, R.T., HAYWARD, R.J., TODD, T.N., et al., in Fusion Technology (Proc. 16th Symp. London, 1990), Vol. 1, Pergamon Press, Oxford (1991) 632.
[9] FITZPATRICK, R., in Theory of Fusion Plasmas (Proc. Joint Varenna-Lausanne Int. Workshop Varenna, 1992), Editrice Compositori, Bologna, in press.
[10] NAVE, M.F.F., WESSON, J.A., Nucl. Fusion **30** (1990) 2575.
[11] WHITE, R.B., MONTICELLO, D.A., ROSENBLUTH, M.N., WADDELL, B.V., Phys. Fluids **20** (1977) 800.
[12] KIM, Y.B., DIAMOND, P.H., GROEBNER, R.J., Phys. Fluids B **3** (1991) 2050.
[13] JOBES, F.C., HOSEA, J.C., in Controlled Fusion and Plasma Physics (Proc. 6th Eur. Conf. Moscow, 1973), Vol. 1, Joint Institute for Nuclear Research, Dubna (1973) 199.
[14] BELL, M.G., Nucl. Fusion **19** (1979) 33.
[15] SUCKEWER, S., EUBANK, H.P., GOLDSTON, R.J., McENERNEY, J., SAUTHOFF, N.R., TOWNER, H.H., Nucl. Fusion **21** (1981) 1301.
[16] HALLOCK, G.A., MATHEW, J., JENNINGS, W.C., HICKOK, R.L., WOOTTON, A.J., ISLER, R.C., Phys. Rev. Lett. **56** (1986) 1248.
[17] BUGARAYA, V.I., GORSHKOV, A.V., GRASHIN, S.A., et al., Nucl. Fusion **25** (1985) 1707.
[18] CHEN, J.Y., McCOOL, S.C., WOOTTON, A.J., et al., in Research Using Small Tokamaks (Proc. Tech. Comm. Mtg Arlington, 1990), IAEA, Vienna (1990) 41.
[19] BUSSAC, M.N., EDERY, D., PELLAT, R., SOULE, J.L., in Plasma Physics and Controlled Nuclear Fusion Research 1976 (Proc. 6th Int. Conf. Berchtesgaden, 1976), Vol. 1, IAEA, Vienna (1977) 607.
[20] CAROLAN, P.G., VALOVIČ, M., BAMFORD, R., et al., in Controlled Fusion and Plasma Physics (Proc. 18th Eur. Conf. Berlin, 1991), Vol. 15C, Part I, European Physical Society (1991) 81.
[21] CHANG, Z., CALLEN, J.D., Nucl. Fusion **30** (1990) 219.
[22] MEREZHKIN, V.G., Sov. J. Plasma Phys. **4** (1978) 152.
[23] SNIPES, J.A., CAMPBELL, D.J., HAYNES, P.S., et al., Nucl. Fusion **28** (1988) 1085.
[24] RUTHERFORD, P.H., Phys. Fluids **16** (1973) 1903.
[25] LAZZARO, E., NAVE, M.F.F., Phys. Fluids **31** (1988) 1623.
[26] WESSON, J.A., SYKES, A., TURNER, M.F., in Plasma Physics and Controlled Nuclear Fusion Research 1984 (Proc. 10th Int. Conf. London, 1984), Vol. 2, IAEA, Vienna (1985) 23.
[27] ROBERTS, D.E., FLETCHER, J.D., NOTHNAGEL, G., et al., in Controlled Fusion and Plasma Heating (Proc. 17th Eur. Conf. Amsterdam, 1990), Vol. 14B, Part I, European Physical Society (1990) 359.
[28] STOTT, P.E., HUGILL, J., FIELDING, S.J., et al., in Controlled Fusion and Plasma Physics (Proc. 8th Eur. Conf. Prague, 1977), Vol. 1, Czechoslovak Academy of Sciences, Prague (1977) 37.
[29] SCOVILLE, J.T., La HAYE, R.J., KELLMAN, A.G., et al., Nucl. Fusion **31** (1991) 875.
[30] FISHPOOL, G.M., CAMPBELL, D.J., FITZPATRICK, R., HAYNES, P.S., in Avoidance and Control of Disruptions in Tokamaks (Proc. Tech. Comm. Mtg Culham, 1991), IAEA, Vienna (1992) 84.
[31] TOSCHI, R., in Plasma Physics and Controlled Nuclear Fusion Research 1990 (Proc. 13th Int. Conf. Washington, DC, 1990), Vol. 3, IAEA, Vienna (1991) 225.
[32] WESSON, J.A., Nucl. Fusion **18** (1978) 87.
[33] HAHM, T.S., KULSRUD, R.M., Phys. Fluids **28** (1985) 2412.
[34] LEE, J.K., IKEZI, H., McCLAIN, F.W., OHYABU, N., Nucl. Fusion **23** (1983) 63.
[35] REIMAN, A., MONTICELLO, D., Phys. Fluids B **3** (1991) 2230.
[36] JENSEN, T.H., LEONARD, A.W., La HAYE, R.J., CHU, M.S., Phys. Fluids B **3** (1991) 1650.
[37] FITZPATRICK, R., HENDER, T.C., Phys. Fluids B **3** (1991) 644.
[38] PERSSON, M., Nucl. Fusion **31** (1991) 382.
[39] PERSSON, M., BONDESON, A., Phys.Fluids B **2** (1990) 2315.
[40] WONG, K.L., PARK, W., Fusion Technol. **12** (1987) 437.
[41] STIX, T.H., Phys. Fluids **16** (1973) 1260.

(Manuscript received 31 December 1991
Final manuscript received 1 October 1992).